DELFT UNIVERSITY OF TECHNOLOGY

SIMULATION, VERIFICATION AND VALIDATION

AE3212-II

Flight Dynamics Assignment - Group B02

Group members	*Student numbers*
Jasper Hemmes	4226216
Karl Martin Kajak	4164806
Robert Koster	4147847
Boris Mulder	4100794
Christel Prins	4197534
Nichsan Rasappu	4204077

March 20, 2015

Contents

Nomenclature

symbol	significance	unit
a	Speed of sound	$\frac{m}{s}$
A	Aspect ratio	m
b	Wing span	m
b_h	Stabiliser span	m
$\bar{c}$	Mean aerodynamic chord length	m
C_{D_0}	Zero lift drag coefficient	(-)
C_ℓ	Roll moment coefficient	(-)
C_L	Lift coefficient	(-)
C_m	Pitching moment coefficient	(-)
$C_{m_{ac}}$	Pitching moment coefficient about the wing's aerodynamic centre	(-)
$C_{X_u}, C_{X_\alpha}, C_{X_{\dot{\alpha}}}, C_{X_q}, C_{X_\delta}$	Force coefficient derivative w.r.t. subscript in longitudinal direction	(-)

$C_{Y_\beta}, C_{Y_{\dot\beta}}, C_{Y_p}, C_{Y_r}, C_{Y_{\delta_a}}, C_{Y_{\delta_r}}$	Force coefficient derivative w.r.t. subscript in lateral direction	(-)
$C_{Z_u}, C_{Z_\alpha}, C_{Z_{\dot\alpha}}, C_{Z_q}, C_{Z_\delta}$	Force coefficient derivative w.r.t. subscript in normal direction	(-)
$C_{m_0}, C_{m_u}, C_{m_\alpha}, C_{\dot\alpha}, C_{m_q}, C_{m_\delta}, C_{m_{T_c}}$	Moment coefficient derivative w.r.t. subscript	(-)
$C_{l_\beta}, C_{l_p}, C_{l_r}, C_{l_{\delta_a}}, C_{l_{\delta_r}}$	Roll moment coefficient derivative w.r.t. subscript	(-)
$C_{n_\beta}, C_{n_{\dot\beta}}, C_{n_p}, C_{n_r}, C_{n_{\delta_a}}, C_{n_{\delta_r}}$	Yaw moment coefficient derivative w.r.t. subscript	(-)
D_b	Dimensionless differential operator of asymmetric motion	(-)
D_c	Dimensionless differential operator of symmetric motion	(-)
e	Oswald factor	(-)
h_p	Pressure altitude	m
h_{p_0}	Initial altitude	m
K_{xz}	Dimensionless product of inertia	(-)
K_{xx}^2	Dimensionless radius of gyration around the X-axis	(-)
l_h	Tail length	m
m	Aircraft mass	kg
$\dot m_f$	Fuel mass flow	$\frac{kg}{s}$
M	Mach number	(-)
M_{ac}	Moment around the aerodynamic center	$N \cdot m$
N	Force in normal direction	N
p	Roll rate	$\frac{rad}{s}$
P	System period	s
q	Pitch rate	$\frac{rad}{s}$
r	Yaw rate	$\frac{rad}{s}$
R	Molar gas constant	$\frac{1}{J \cdot \text{mol} \cdot K}$
Re	Reynolds number	(-)
S	Wing surface area	m^2
T	Force in tangential direction	N
$T_{\frac{1}{2}}$	Half amplitude time	s
T_P	Thrust	N
$\hat u$	Non-dimensional speed difference with respect to trim speed at stable flight condition	(-)
u	Deviation of the true airspeed with the initial true airspeed	$\frac{m}{s}$
V_{CAS}	Calibrated air speed	$\frac{m}{s}$
V_{TAS}	True air speed	$\frac{m}{s}$
V_0	Initial true airspeed	$\frac{m}{s}$
W	Aircraft weight	N
α	Angle of attack	$^\circ$
α_0	Initial angle of attack	$^\circ$
$\dot\alpha$	Derivative of the angle of attack w.r.t. time	$\frac{^\circ}{s}$
β	Angle of slide slip	$^\circ$
$\dot\beta$	Derivative of the angle of slide w.r.t. time	$\frac{^\circ}{s}$
γ	adiabatic index	(-)
δ	Natural logarithm of ratio of two consecutive maxima	(-)
δ_a	Aileron deflection angle	$^\circ$
δ_e	Elevator deflection angle	$^\circ$
δ_r	Rudder deflection angle	$^\circ$
ζ	Damping ratio	(-)
λ	Eigenvalue	(-)
μ	Dynamic viscosity	$\frac{kg}{m \cdot s}$
μ_b	Relative density of asymmmetric motion	(-)
μ_c	Relative density of symmmetric motion	(-)
ξ	Damping coefficient	(-)
ρ	Air density	$\frac{kg}{m^3}$
φ	Roll angle	$^\circ$
θ	Pitch angle	$^\circ$
θ_0	Initial pitch angle	$^\circ$
ω_d	Damped frequency	$\frac{\text{rad}}{s}$
ω_n	Natural frecuency	$\frac{\text{rad}}{s}$

1. Introduction

Worldwide air plane manufacturers are designing new air planes including business jets. Just like all air planes, business jets must be designed for stability. The best way to check whether a design meets the stability requirements is building and testing the design. However, this method is not feasible because it would be too expensive to build many prototypes and there is too much risk for the test pilots. Therefore, simulation models are built instead in order to determine the dynamic behaviour of new aircraft designs. Such tools shouldn't only be built, but also

verified and validated to guarantee useful results. It is not only important to built simulation tools but also to come up with verification and validation methods to improve the simulation tool and/or guarantee proper functioning. A simulation plan has been made prior to this report with propositions on how to create the simulation tool. In this simulation plan flowcharts for the simulation tool are presented. These flow charts are used as a guideline to set up the simulation program.

The purpose of this report is to present the created simulation tool and its results. The problem statement for this tool is: *what is the dynamic response of an aircraft to disturbances and control inputs?* The method used to design the simulation model is as proposed in the simulation plan.

This report is structured as follows. Chapter 2 covers the analysis of the problem: the main problem, the input and output variables of the simulation tool, the general assumptions and the reference frames are all stated. In chapter 3 the analytical solution for the dynamic response is stated, also the analytical methods used to process the data of the first and second measurement series is stated. The same is done in chapter 4 for the numerical methods, this chapter also contains overviews of the programs used. The verification and validation of the simulation model will be covered in chapters 5 and 6 respectively. Finally in chapter 7 a final discussion of the program is presented with advice on possible improvements on the model.

2. Problem analysis

This chapter analyses the problem stated in the introduction. The input and output variables in section 2.2. The assumptions used and their effects on the solutions can be found in 2.3 and the reference frame used is described in 2.4.

2.1 Main problem

For the further development of a new aircraft, of which currently only a prototype is available, a simulation tool is required. Thus, a preliminary tool must built to predict the behaviour of the prototype using the known design parameters of the prototype. However, not all of those parameters are accurate and therefore this prediction won't be very accurate either. Therefore, a flight test, consisting of both static as well as dynamic tests, must be performed with the prototype. From the static test data certain parameters of the preliminary simulation tool can be improved and so the prediction should become more accurate as well. Using the dynamic test data the improved simulation tool can be validated to determine whether it is useful for further development of the new aircraft.

2.2 Input and output variables

There are two input sets for the simulation model, the inputs for the symmetrical and the asymmetrical case. The inputs of the state-space system can be found in table 2.1. The general variables are used for both cases. For the symmetrical case the longitudinal force derivatives, normal force derivatives and pitch moment derivatives are used. For asymmetrical case the lateral force derivatives, roll moment derivatives and lateral force derivatives are used.

The data gathered from the two flight test measurement series is used to calculate some important variables to improve the accuracy of the simulation. This input data is found in table 2.2.

For the outputs there are 3 variable sets. These three outputs are for the state-space system and the measurement series 1 and 2. The output variables can be found in table 2.3.

Table 2.1: Input variables of the state-space systems

Category	**variables**
General variables	$\hat{u}$, θ, q, $\bar{c}$, V, K_{xx}^2, K_{yy}^2, K_{zz}^2, K_{xz}^2, μ_c
Longitudinal force derivatives	C_{X_u}, C_{X_α}, $C_{X_{\dot{\alpha}}}$, C_{X_q}, C_{X_δ}
Normal force derivatives	C_{Z_u}, C_{Z_α}, $C_{Z_{\dot{\alpha}}}$, C_{Z_q}, C_{Z_δ}
Pitch moment derivatives	C_{m_0}, C_{m_u}, C_{m_α}, $C_{\dot{\alpha}}$, C_{m_q}, C_{m_δ}, $C_{m_{T_c}}$
Lateral force derivatives	C_{Y_β}, $C_{Y_{\dot{\beta}}}$, C_{Y_p}, C_{Y_r}, $C_{Y_{\delta_a}}$, $C_{Y_{\delta_r}}$
Roll moment derivatives	C_{l_β}, C_{l_p}, C_{l_r}, $C_{l_{\delta_a}}$, $C_{l_{\delta_r}}$
Yaw force derivatives	C_{n_β}, $C_{n_{\dot{\beta}}}$, C_{n_p}, C_{n_r}, $C_{n_{\delta_a}}$, $C_{n_{\delta_r}}$

Table 2.2: Input variables for the measurements

Category	**variables**
General Aircraft Parameters	S, b, A, c, W_{empty}
(ISA) standard vaules	ρ_0, λ, T_0, g_0, R, $gamma$, p_0
Measurement I	h_p, V_{CAS}, V_{TAS}, F_{fr}, F_{fl}, $W_{fuelused}$, $W_{fuelstart}$, $W_{payload}$, α, T_m,
Measurement II	α, V, h, W_f, T, F_{fr}, F_{fl}, δ_e

Table 2.3: Output variables

Output set	variables
State-space model	$V_t(t)$, $\theta(t)$, $\alpha(t)$, $\beta(t)$, $\phi(t)$, $p(t)$, $q(t)$, $r(t)$, λ_a, λ_s
First measurement series	$C_L^2(C_D)$, $C_L(C_D)$, $C_L(\alpha)$, $C_D(\alpha)$, C_{D_0}, e, Re, M, X_{cg}
Second measurement series	C_{m_δ}, C_{m_α}, $\delta^*_{e_{eq}}(\tilde{V}_e)$, $F_e(\tilde{V}_e)$

2.3 General assumptions

Assumptions are used to simplify equations that will be used in the analytical and numerical solutions. The assumption are classified in primary or secondary. Primary means the assumptions has a large impact on the solution. Secondary means that it has minor impact on the solution. The general assumptions that have been made are described below.

2.3.1 Primary assumptions

- It is assumed there is no wind which means that the wind is at rest w.r.t. the earth's surface. In real flight there can be significant disturbances in the airflow, affecting the forces on the aircraft.
- For this tool it is assumed that the aircraft has a conventional configuration. The aircraft has a wing with ailerons, a aft horizontal stabilizer with an elevator and an aft vertical stabilizer with a rudder. The calculations only apply to this situation.
- It is assumed that the aircraft has a rigid body with a constant mass, while in reality the aircraft will deform which changes the matrices of inertia as well as the forces on the lifting surfaces.
- It is assumed the Earth is flat as opposed to elliptical. This means that the earth's reference frame does not rotate due to the curvature of the Earth.
- It is assumed that the Earth non-rotating. The reference frame will always have the same rotation to the body reference frame. This is a primary assumption as the Earth rotates in reality.

2.3.2 Secondary assumptions

- The aircraft is considered to have a plane of symmetry. Of course this is not the case, but the aerodynamic interference caused by the asymmetric appendage is negligible.
- It is assumed that the thrust of the engine will only have an influence on the symmetric aerodynamic forces X,Z and the symmetric aerodynamic moment M. Having a Y component of thrust is specifically avoided in design, so the impact should be negligible.

2.4 Reference frame

The reference frame used for deriving all equations can be found in figures 2.1, 2.3 and 2.2. Figure 2.1 gives the top view, figure 2.3 gives the front view and figure 2.2 gives the side view of the aircraft. Three reference systems are used to determine the EOM. The reference systems are the body fixed, aerodynamic and vehicle carried normal earth reference system indicated with the subscript b, a and e respectively.

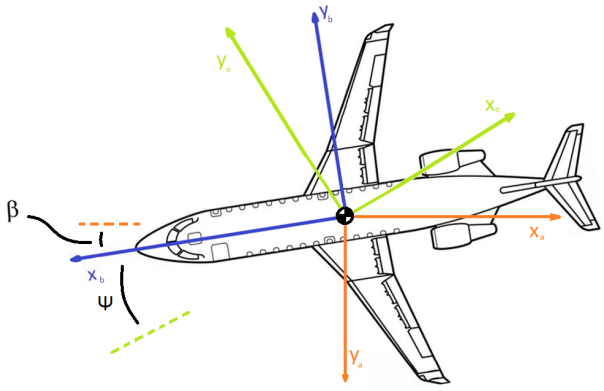

Figure 2.1: Reference frames projected on top view of aircraft

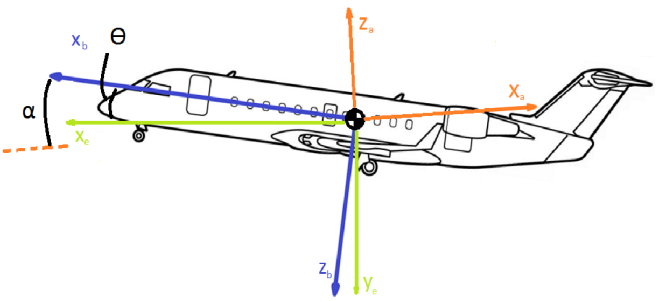

Figure 2.2: Reference frames projected on side view of aircraft

3. Analytical solution

This chapter covers the analytical solution used to describe the response model of the aircraft and the analytical solutions for the data processing of the first and second measurement series. The equations of motion are covered in section 3.2. The equilibrium equations for horizontal, stationary and symmetric flight are given in section 3.1.

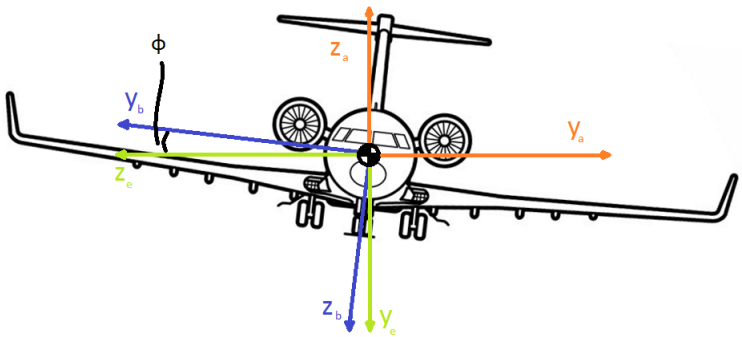

Figure 2.3: Reference frames projected on front view of aircraft

The profile drag coefficient C_{D_0}, the Oswald factor e, the lift gradient C_{L_α}, the longitudinal stability C_{M_α} and the elevator effectiveness $C_{M_{\delta_e}}$ will be corrected according to the two sets of measurement data collected during the flight test. The programs necessary to facilitate this correction are presented in sections 3.3 and 3.4.

The assumptions holding for the equations presented in this section are detailed in section 3.5.

3.1 Equilibrium equations for horizontal, stationary and symmetric flight

This section gives the basic equilibrium equations for horizontal, stationary and symmetric flight. Figure 3.1 shows all possible forces and moments applied to an aircraft. Note that the axis system is inconsequentially different from the reference frame described in section 2.4. The equilibrium equations are established for the forces along the X- and Z-axis and for moments about the Y-axis resulting in equations 3.1, 3.2 and 3.3

$$T_w + T_h - T_p cos(i_p) + N_p sin(i_p) = -W sin(\theta) \tag{3.1}$$

$$N_w + N_h - N_p cos(i_p) + T_p sin(i_p) = W cos(\theta) \tag{3.2}$$

$$\begin{aligned} &M_{ac_w} + N_w(x_{cg} - x_w) - T_w(z_{cg} - z_w) + M_{ac_h} + N_h(x_{cg} - x_h) - T_h(z_{cg} - z_h) \\ &+(N_p cos(i_p) + T_p sin(i_p))(x_{cg} - x_p) + (T_p cos(i_p) - N_p sin(i_p))(z_{cg} - z_p) = 0 \end{aligned} \tag{3.3}$$

To simplify these 3 equations, first it is assumed that $i_p = 0$, which means that $-T_p cos(i_p) + N_p sin(i_p) = -T_p$. Then, by substituting the expressions for T_w, T_h, T_p, N_p, N_w, N_h, M_{ac_w} and M_{ac_h} as given in [4] and then dividing the force equilibrium equations by $\frac{1}{2}\rho V^2 S$ and the moment equilibrium equation by $\frac{1}{2}\rho V^2 S\bar{c}$ the dimensionless force and moment equilibrium equations can be obtained. Furthermore, by assuming a gliding flight T_p and N_p can be neglected for all 3 equilibrium equations. The contribution of T_h in the force equation in X-direction and of T_w to the moment equation are assumed to be negligible. Finally, it is assumed that the tail plane has a symmetric airfoil due to which $M_{ac_h} = 0$. Due to these assumptions the equilibrium equations reduce to equations 3.4, 3.5 and 3.6.

$$C_{T_w} = -\frac{W}{\frac{1}{2}\rho V^2 S} sin(\theta) \tag{3.4}$$

$$C_{N_w} + C_{N_h}(\frac{V_h}{V})^2 \frac{S_h}{S} = \frac{W}{\frac{1}{2}\rho V^2 S} cos(\theta) \tag{3.5}$$

$$C_{m_{ac_w}} + C_{N_w}\frac{x_{c.g.} - x_w}{\bar{c}} + C_{N_h}(\frac{V_h}{V})^2 \frac{S_h}{S}\frac{x_{c.g.} - x_h}{\bar{c}} = 0 \tag{3.6}$$

3.2 Equations of motion for the simulation

Matrix equations 3.7 [4] and 3.8 [4] describe the response of an aircraft to disturbances and control inputs for symmetric and asymmetric flight, respectively.

Equation 3.7 describes the linear motions along the X and the Z axis and the rotational motion around the Y axis as defined by the reference system in chapter 2. These motions are described by the state variables $\hat{u}$ (the dimensionless speed u/V_0, where V_0 is the true airspeed in stationary nominal condition and u is the absolute deviation of the current true airspeed from V_0), α (the angle of attack), θ (the pitch angle) and q (the pitch rate) and by the elevator deflection δ_e as control input. The rest of the parameters in the matrices are dependent on the aerodynamic and geometric characteristics of the aircraft and are inputs of the simulation model.

Equation 3.8 describes the linear motion along the Y axis and the rotational motions around the X and Z axis. In this case the state variables are β (the side slip angle), ϕ (the roll angle), p (the roll rate) and r (the yaw rate) and the control inputs are δ_e (the aileron deflection) and δ_r (the rudder deflection).

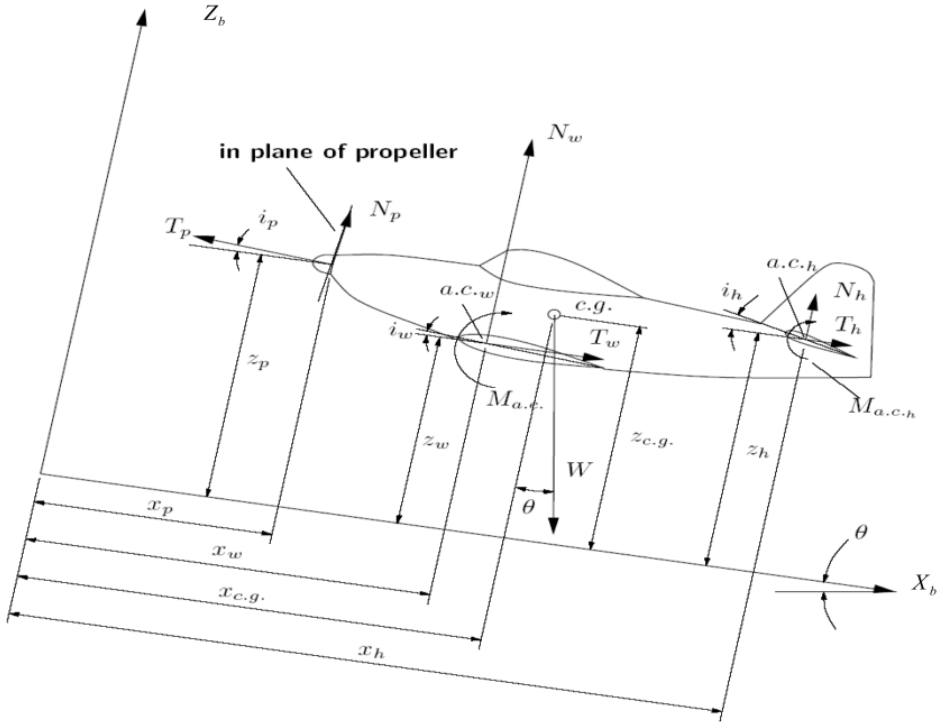

Figure 3.1: Aircraft with all the possible forces and moments. [4]

$$\begin{bmatrix} C_{X_U}-2\mu_c D_c & C_{X_\alpha} & C_{Z_0} & C_{X_q} \\ C_{Z_u} & C_{Z_\alpha}+\left(C_{Z_{\dot\alpha}}-2\mu_c\right)D_c & -C_{X_0} & C_{Z_q}+2\mu_c \\ 0 & 0 & -D_c & 1 \\ C_{m_u} & C_{m_\alpha}+C_{m_{\dot\alpha}}D_c & 0 & C_{m_q}-2\mu_c K_Y^2 D_c \end{bmatrix} \cdot \begin{bmatrix} \hat{u} \\ \alpha \\ \theta \\ \frac{q\bar{c}}{V_0} \end{bmatrix} = \begin{bmatrix} -C_{X_{\delta_e}} \\ -C_{Z_{\delta_e}} \\ 0 \\ -C_{m_{\delta_e}} \end{bmatrix} \cdot \delta_e \tag{3.7}$$

$$\begin{bmatrix} C_{Y_\beta}+\left(C_{Y_{\dot\beta}}-2\mu_b\right)D_b & C_L & C_{Y_p} & C_{Y_r}-4\mu_b \\ 0 & -\frac{1}{2}D_b & 1 & 0 \\ C_{\ell_\beta} & 0 & C_{\ell_p}-4\mu_b K_X^2 D_b & C_{\ell_r}+4\mu_b K_{XZ} D_b \\ C_{n_\beta}+C_{n_{\dot\beta}}D_b & 0 & C_{n_p}+4\mu_b K_{XZ} D_b & C_{n_r}-4\mu_b K_Z^2 D_b \end{bmatrix} \cdot \begin{bmatrix} \beta \\ \varphi \\ \frac{pb}{2V_0} \\ \frac{rb}{2V_0} \end{bmatrix} = \begin{bmatrix} -C_{Y_{\delta_a}} \\ 0 \\ -C_{\ell_{\delta_a}} \\ -C_{n_{\delta_a}} \end{bmatrix} \cdot \delta_a + \begin{bmatrix} -C_{Y_{\delta_r}} \\ 0 \\ -C_{\ell_{\delta_r}} \\ -C_{n_{\delta_r}} \end{bmatrix} \cdot \delta_r \tag{3.8}$$

3.2.1 Solution of the eigenmotions

This section presents the calculation of the eigenvalues for the eigenmotions of the aircraft. For each flight mode the assumptions to simplify the A matrices are stated first, then the simplified matrix is solved for the eigenvalues. The resulting eigenvalues are presented and discussed at the end of this section.

The matrices A_s and A_a are given in equation 3.9 and 3.10 respectively. To calculate the eigenvalues, D_c and D_b in the matrices are substituted by λ_c and λ_b respectively. Then the determinant of this matrix is set equal to zero to determine the eigenvalues.

$$A_s = \begin{bmatrix} C_{X_U}-2\mu_c D_c & C_{X_\alpha} & C_{Z_0} & C_{X_q} \\ C_{Z_u} & C_{Z_\alpha}+\left(C_{Z_{\dot\alpha}}-2\mu_c\right)D_c & -C_{X_0} & C_{Z_q}+2\mu_c \\ 0 & 0 & -D_c & 1 \\ C_{m_u} & C_{m_\alpha}+C_{m_{\dot\alpha}}D_c & 0 & C_{m_q}-2\mu_c K_Y^2 D_c \end{bmatrix} \tag{3.9}$$

$$A_a = \begin{bmatrix} C_{Y_\beta}+\left(C_{Y_{\dot\beta}}-2\mu_b\right)D_b & C_L & C_{Y_p} & C_{Y_r}-4\mu_b \\ 0 & -\frac{1}{2}D_b & 1 & 0 \\ C_{\ell_\beta} & 0 & C_{\ell_p}-4\mu_b K_X^2 D_b & C_{\ell_r}+4\mu_b K_{XZ} D_b \\ C_{n_\beta}+C_{n_{\dot\beta}}D_b & 0 & C_{n_p}+4\mu_b K_{XZ} D_b & C_{n_r}-4\mu_b K_Z^2 D_b \end{bmatrix} \tag{3.10}$$

Short period oscillation

To calculate the eigenvalues for this motion the matrix A_s that is given in equation 3.9 is used. The first assumption is that the airspeed remains constant during this motion. Furthermore the flight condition prior to the motion is assumed to be steady, level flight. Because this eigenmotion only occurs over a short time interval, the effect of the assumptions will be small. Using these assumptions the matrix A_s can be simplified to equation 3.11. Substituting D_c for λ_c and then taking the determinant of this matrix 3.11 and equate that to zero will give equation 3.12. The roots of equation 3.12 will give the complex eigenvalues of this motion. [4]

$$A_s = \begin{bmatrix} C_{Z_\alpha} + \left(C_{Z_{\dot{\alpha}}} - 2\mu_c\right) D_c & C_{Z_q} + 2\mu_c \\ C_{m_\alpha} + C_{m_{\dot{\alpha}}} & C_{m_q} - 2\mu_c {K_Y}^2 D_c \end{bmatrix} \tag{3.11}$$

$$\left[\left(2\mu_c - C_{Z_{\dot{\alpha}}}\right) 2\mu_c K_Y^2\right] \cdot \lambda_c^2 + \left[\left(C_{Z_{\dot{\alpha}}} - 2\mu_c\right) C_{m_q} - \left(C_{Z_q} + 2\mu_c\right) C_{m_{\dot{\alpha}}} - C_{Z_\alpha} 2\mu_c K_Y^2\right] \cdot \lambda_c + C_{Z_q} C_{m_q} - \left(C_{Z_q} + 2\mu_c\right) C_{m_\alpha} = 0 \tag{3.12}$$

Phugoid

For this motion it is assumed that the variations in angle of attack occur slowly, so the contribution of $\dot{\alpha}$ is negligible. Secondly it is assumed that the pitch rate is constant. The previous two assumptions will most likely increase the damping, and since the phugoid is an eigenmotion that exists for a long period, it is assumed that these assumptions will have a rather large impact on the resulting eigenvalues. Finally it is assumed that the initial flight condition is steady. These assumptions reduce the matrix given in 3.9 to the matrix in equation 3.13. Then setting the determinant of matrix 3.13 equal to zero gives equation 3.14, the roots of this equation will give the eigenvalues of this flight mode. Finally the roots of equation 3.14 give the eigenvalues for this flight mode. [4]

$$A_s = \begin{bmatrix} C_{X_u} - 2\mu_c D_c & C_{X_\alpha} & C_{Z_0} & 0 \\ C_{Z_u} & C_{Z_\alpha} & 0 & 2\mu_c \\ 0 & 0 & -D_c & 1 \\ C_{m_u} & C_{m_\alpha} & 0 & C_{m_q} \end{bmatrix} \tag{3.13}$$

$$\left[2\mu_c C_{Z_\alpha} C_{m_q} - 4\mu_c^2 C_{m_\alpha}\right] \cdot \lambda_c^2 + \left[\left(C_{X_\alpha} C_{Z_u} - C_{X_u} C_{Z_\alpha}\right) C_{m_q} + \left(C_{X_u} C_{m_\alpha} - C_{X_\alpha} C_{m_u}\right) 2\mu_c\right] \cdot \lambda_c + \left(C_{Z_\alpha} C_{m_u} - C_{Z_u} C_{m_\alpha}\right) C_{z_0} = 0 \tag{3.14}$$

Aperiodic roll

For this eigenmotion it is assumed that the aircraft can only roll about the longitudinal axis. From this assumption it results that $\beta = \frac{rb}{2V} = 0$. In the remaining equation the angle of roll is no longer necessary, using these assumptions matix $eq : Aa$ is reduces to the equation for the rolling moment, which is given in equation 3.15. From 3.15 the real eigenvalue can be easily found, and this eigenvalue is given in equation 3.16. [4]

$$\left(C_{\ell_p} - 4\mu_b K_X^2 D_b\right) \frac{pb}{2V} = 0 \tag{3.15}$$

$$\lambda_b = \frac{C_{\ell_p}}{4\mu_b K_X^2} \tag{3.16}$$

Dutch roll

For the simplification of matrix A_a from equation 3.10 it is firstly assumed that the rolling component can be neglected. This sets φ and $\frac{pb}{2V}$ to zero. Then also the rolling moment can be neglected since this rolling moment should remain balanced. Also the contributions of $C_{Y_{\dot{\beta}}}$ are $C_{n_{\dot{\beta}}}$ neglected since these values are very small, as well as C_{Y_r} which is neglected because this value is insignificant compared to $2\mu_b$. These assumptions and simplifications reduce matrix A_a to the matrix in equation 3.17. Then equating the determinant of this simplified matrix to zero gives equation 3.18, of which the roots will be the eigenvalues for this motion. [4]

$$A_a = \begin{bmatrix} C_{Y_\beta} - 2\mu_b D_b & -4\mu_b \\ C_{n_\beta} & C_{n_r} - 4\mu_b K_Z^2 D_b \end{bmatrix} \tag{3.17}$$

$$\left[8\mu_b^2 K_Z^2\right] \cdot \lambda_b^2 + \left[-\left(4C_{Y_\beta} K_Z^2 + 2C_{n_r}\right) \mu_b\right] \cdot \lambda_b + C_{Y_\beta} C_{n_r} + 4\mu_b C_{n_\beta} \tag{3.18}$$

Aperiodic spiral

The first assumption made is that all linear and angular accelerations are zero, i.e. $D_b\beta = D_b \frac{pb}{2V} = D_b = \frac{rb}{2V} = 0$. This is a valid assumption since this is a very slow eigenmotion. Also it is assumed that C_{Y_r} and C_{Y_p} are negligible, so these will be left out of the equation. This reduces matrix A_a to equation 3.19. Then using the determinant of this matrix the solution for the eigenvalue can be found and is shown in equation 3.20. [4]

$$A_a = \begin{bmatrix} C_{Y_\beta} & C_L & 0 & -4\mu_b \\ 0 & -\frac{1}{2}D_b & 1 & 0 \\ C_{\ell_\beta} & 0 & C_{\ell_p} & C_{\ell_r} \\ C_{n_\beta} & 0 & C_{n_p} & C_{n_r} \end{bmatrix} \tag{3.19}$$

$$\lambda_b = \frac{\left(C_{\ell_\beta}C_{n_r} - C_{n_\beta}C_{\ell_r}\right)2C_L}{\left(C_{Y_b}C_{n_r} + 4\mu_b C_{n_\beta}\right)C_{\ell_p} - \left(C_{Y_\beta}C_{\ell_r} + 4\mu_b C_{\ell_\beta}\right)C_{n_p}} \tag{3.20}$$

Dutch roll and aperiodic roll

For this flight mode it is assumed that the center of gravity moves along a straight line, while rolling motion is permitted. This removes the Y equation. The resulting matrix in ψ and $\frac{pb}{2V}$ can be seen in equation 3.21. The determinant of this equation gives equation 3.22. [4]

$$A_a = \begin{bmatrix} -C_{\ell_\beta} + \frac{1}{2}C_{\ell_r}D_b + 2\mu_b K_{XZ}D_b^2 & C_{\ell_p} - 4\mu_b K_X^2 D_b \\ -C_{n_\beta} + \frac{1}{2}C_{n_r}D_b - 2\mu_b K_Z^2 D_b^2 & C_{n_p} + 4\mu_b K_{XZ}D_b \end{bmatrix} \tag{3.21}$$

$$\begin{aligned}\left[\left(K_X^2K_Z^2 - K_{XZ}^2\right)4\mu_b^2\right]\cdot\lambda_b^3 + \left[-\left\{C_{n_r}K_X^2 + C_{\ell_p}K_Z^2 + \left(C_{\ell_r} + C_{n_p}\right)K_{XZ}\right\}2\mu_b\right]\cdot\lambda_b^2 \\ + \left[\left(C_{\ell_\beta}K_{XZ} + C_{n_\beta}K_X^2\right)2\mu_b + \frac{1}{4}\left(C_{\ell_p}C_{n_r} - C_{n_p}C_{\ell_r}\right)\right]\cdot\lambda_b + \frac{1}{2}\left(C_{\ell_\beta}C_{n_p} - C_{n_\beta}C_{\ell_p}\right) = 0\end{aligned} \tag{3.22}$$

Results

- **Short period**, $\lambda_{c_{1,2}} = -0.02789 \pm 0.04333i$
- **Phugoid**, $\lambda_{c_{1,2}} = -0.0001410 \pm 0.002679i$
- **Aperiodic roll**, $\lambda_b = -0.6764$
- **Dutch roll**, $\lambda_{b_{1,2}} = -0.05792 \pm 0.3393i$
- **Aperiodic spiral**, $\lambda_b = 0.001630$
- **Dutch roll and aperiodic roll**, $\lambda_{b_{1,2}} = 0.05390 \pm 0.1280i; \lambda_{b_3} = -0.1306$

The eigenvalues resulting from the analytical solution are in the form that is expected, also the order of magnitude is similar to the eigenvalues calculated in [4] which are assumed to be correct. As can be seen the short period, phugoid, aperiodic roll and dutch roll all have a negative real part, this is exactly as expected since a negative real part means stability. Another interesting result is that when comparing the Short period and Phugoid it can be seen that the phugoid has a smaller imaginary part, which results in a larger period than the short period eigenmotion. Furthermore can be seen that the aperiodic spiral has a very small positive eigenvalue. This also makes sense because the spiral is not stable, the small value means that it takes very long to move away from equilibrium position which is also true. Finally it can be seen that the Dutch roll combined with an aperiodic roll generates three eigenvalues, this due to the third order polynomial in this calculation.

3.2.2 Equilibrium conditions

For the matrices of the previous section the two dimensionless equilibrium conditions X_0 and Z_0 have to be calculated separately, as shown in equations 3.23 and 3.24 [4]. The aircraft mass, the air density and the trim speed are not known variables. A function that calculates the aircraft weight is given in section 3.3.2. Air density is calculated using 3.3.2. Trim speed is calculated using equation 3.32. These calculations process the measurements taken during trimmed flight.

$$C_{X_0} = \frac{W\sin(\theta_0)}{\frac{1}{2}\rho V_{t_0}^2 S} \tag{3.23}$$

$$C_{Z_0} = -\frac{W\cos(\theta_0)}{\frac{1}{2}\rho V_{t_0}^2 S} \tag{3.24}$$

3.3 First measurement series

The first measurement series gives the tools to derive several aerodynamic properties. It can be used to correct initial values for the Oswald factor e, the zero lift drag-coefficient C_{D_0} and the slope of the lift curve C_{L_α}.

The $C_L^2 - C_D$, $C_L - \alpha$, $C_D - \alpha$ and $C_L - C_D$ curves in two configurations can be found from the first measurement series, but to create these curves the values of C_L and C_D have to be found. C_L can be found using equation 3.25, where $C_L \approx C_N$ due to the small angle assumption. C_D can be found using equation 3.26.

$$C_L = \frac{2W}{\rho V_{TAS}^2 S} = C_{L\alpha}(\alpha - \alpha_0) \approx C_{N\alpha}(\alpha - \alpha_0) \quad (3.25)$$

$$C_D = \frac{2T_p}{\rho V_{TAS}^2 S} = C_{D_0} + \frac{{C_L}^2}{\pi A e} \quad (3.26)$$

The C_L and C_D equations require the true airspeed V_{TAS}, the air density ρ and wing area. The wing area is a known aircraft parameter. True airspeed and the air density are calculated instantaneously, as explained in section 3.3.1.

To calculate C_L, the instantaneous weight of the aircraft has to be calculated as explained in section 3.3.2. To calculate C_D the engine thrust has to be calculated as explained in section 3.3.3.

The Reynolds number to describe the airflow is given by equation 3.27. The dynamic viscosity μ can be calculated using equation 3.28 [5]. Where T is the temperature in Kelvin.

$$Re = \frac{\rho V_{TAS} c}{\mu} \quad (3.27)$$

$$\mu = \frac{1.458 \cdot 10^{-6} T^{\frac{3}{2}}}{T + 110.4} \quad (3.28)$$

3.3.1 True airspeed and air density

The calibrated airspeed V_{CAS} measured by the aircraft has to be converted to true airspeed V_{TAS}. Equation 3.29 is used to calculate air pressure at pressure altitude h_p. The pressure is then used to calculate the Mach number M in equation 3.30. The speed of sound a is determined from equation 3.31, which is then used to calculate V_{TAS} with equation 3.32. In equation 3.31 T is the static air temperature, which follows from the measured temperature T_m and equation 3.33. Air density ρ is calculated using equation 3.34.

$$p = p_0 (1 + \frac{\lambda h_p}{T_0})^{-\frac{g_0}{\lambda R}} \quad (3.29)$$

$$M = \sqrt{\frac{2}{\gamma - 1}\left(\left(1 + \frac{p_0}{p}\left(\left(1 + \frac{\gamma - 1}{2\gamma}\frac{\rho_0}{p_0}V_c^2\right)^{\frac{\gamma}{\gamma-1}} - 1\right)\right)^{\frac{\gamma-1}{\gamma}} - 1\right)} \quad (3.30)$$

$$a = \sqrt{\gamma R T} \quad (3.31)$$

$$V_{TAS} = Ma \quad (3.32)$$

$$T = \frac{T_m}{1 + \frac{\gamma-1}{2}M^2} \quad (3.33)$$

$$\rho = \frac{p}{RT} \quad (3.34)$$

3.3.2 Weight function

The instantaneous weight of the aircraft is calculated using equation 3.35 [4]. The weight is determined before lift-off by summing total fuel weight, weight of the passengers and known aircraft empty weight.

$$W(t) = rampweight - g_0 \int_0^{t_1} \dot{m}_{f_{\lambda+r}} dt \quad (3.35)$$

3.3.3 Thrust calculation

The thrust is calculated using `thrust.exe`. Its underlying theory is explained in this section.

Thrust is defined by equation 3.36. Substituting equation 3.37 for η_{tot} into equation 3.36 simplifies equation 3.36 to equation 3.38.

This expression is simplified using several assumptions. Firstly, it is implicitly assumed that H and η_{tot} are constant, also it is assumed that the ratio between $\dot{m}$ and $\dot{m}_f$ remains constant during flight. Furthermore, V_0 is substituted with the mach number of the undisturbed flow M_0 as in equation 3.39. Lastly, p_0 is replaced with the pressure altitude h_p. These substitutions and assumptions cause the equation for the thrust to be dependant on only three variables, as can be seen in equation 3.40

$$T_p = \frac{\eta_{tot} \dot{m}_f H}{V_0} \quad (3.36)$$

$$\eta_{tot} = \frac{T_p V_0}{\dot{m}_f H} \quad (3.37)$$

$$T_p = \dot{m}(\bar{w}_e - V_0) = f\left(\eta_{tot}, \dot{m}_f, H, V_0, \dot{m}\right) \tag{3.38}$$

$$M_0 = V_0\sqrt{\gamma R T_0} \tag{3.39}$$

$$T_p = f\left(\dot{m}_f, h_p, M_0\right) \tag{3.40}$$

3.3.4 Results of first measurement series

The analytical results of the first measurement series can be found in table 3.1. The calculation of thrust with `thrust.exe` was treated as a verified and valid calculation.

Table 3.1: Input and output variables for analytically calculated variables for first measurement series

Input		
Variable	Value	Unit
T_0	288	K
g_0	9.81	$\frac{m}{s^2}$
γ	1.4	$-$
h_p	$2.145 \cdot 10^3$	m
p_0	101325	Pa
λ	-0.0065	$\frac{K}{m}$
V_{CAS}	130.6689	$\frac{m}{s}$
ρ_0	1.225	$\frac{kg}{m^3}$
R	287.05	$\frac{J}{kg \cdot K}$
W_r	$6.12 \cdot 10^4$	kg
$F_u sed$	175.0876	kg
(c)	2.569	m
S	30	m^2
$Thrust$	$7.3287 \cdot 10^3$	N

Output		
Variable	Value	Unit
p	78049	Pa
M	0.433	$-$
T	276.96	K
a	334.62	$\frac{m}{s}$
dT	2.91	K
V_{TAS}	145.44	$\frac{m}{s}$
ρ	0.98173	$\frac{kg}{m}$
W	$6.1058 \cdot 10^4$	kg
c_D	0.024	$-$
c_L	0.196	$-$
Re	$1.6928 \cdot 10^7$	$-$

3.3.5 Discussion of results

The output variables of table 3.1 are calculated for only one measurement point. These are compared to the same measurement point for verification in chapter 5. The output values are as expected. The pressure p at altitude h_p is smaller than the pressure p_0, which is in line with the ISA, the temperature T, the speed of sound a and the density ρ also went down as expected. The mach number makes sense as the Citation can fly up to 0.7 mach [2] and the aircraft was not flying near full speed. It was also flying at a lower altitude as the 0.7 mach measurement so the speed of sound was higher. The V_{TAS} is slightly higher than the V_{CAS}, it is known that these values should be fairly close together, which they are as was hypothesised. The weight of the aircraft decreases due to fuel consumption - this is the case. The C_L and C_D values are low as expected due to the small angle of attack of 1.1 degrees.

3.4 Second measurement series

The longitudinal stability, C_{m_α}, and the elevator effectiveness, C_{m_δ}, are determined using the second measurement series data to improve the simulation model. Moreover, the static stability of the aircraft is investigated by setting up and analyzing the elevator trim curve and the elevator control force curve. Before setting up these curves the measurement data must be reduced to standard conditions, making them comparable to other flights. The calculation of the reduced elevator deflection and elevator control force are explained in sections 3.4.1 and 3.4.2, respectively. The calculation of C_{m_α} and C_{m_δ} are given in sections 3.4.3 and 3.4.5, respectively.

3.4.1 Reduced elevator deflection

The elevator trim deflection is given by equation 3.41 [4]. To reduce this equation to standard conditions, first equation 3.25 is inserted resulting in equation 3.42. Under the assumption that measurement errors are negligible, this equation gives the measured elevator deflection, $\delta_{e_{meas}}$.

$$\delta_e = -\frac{1}{C_{m_\delta}}\left(C_{m_0} + C_{m_\alpha}(\alpha - \alpha_0) + C_{m_{\delta_f}}\delta_f + C_{m_{T_c}}T_c + C_{m_{lg}}|_{lgdown}\right) \tag{3.41}$$

$$\delta_e = -\frac{1}{C_{m_\delta}}\left(C_{m_0} + \frac{C_{m_\alpha}}{C_{N_\alpha}}\frac{2W}{\rho V_{TAS}^2 S} + C_{m_{\delta_f}}\delta_f + C_{m_{T_c}}T_c + C_{m_{lg}}|_{lgdown}\right) \tag{3.42}$$

The true airspeed, V_{TAS} can converted to equivalent airspeed using equation 3.43, which can then be converted to reduced equivalent airspeed by reducing the weight W to the standard weight W_s with equation 3.44, resulting in equation 3.45.

$$V_e = V_{TAS}\sqrt{\frac{\rho}{\rho_0}} \tag{3.43}$$

$$\widetilde{V_e} = V_e\sqrt{\frac{W_s}{W}} \tag{3.44}$$

$$\delta_e^* = -\frac{1}{C_{m_\delta}}\left(C_{m_0} + \frac{C_{m_\alpha}}{C_{N_\alpha}}\frac{2W}{\rho\widetilde{V_e}^2 S} + C_{m_{\delta_f}}\delta_f + C_{m_{T_{c_s}}}T_{c_s} + C_{m_{lg}}|_{lgdown}\right) \tag{3.45}$$

It can be seen that equation 3.45 is related to 3.42 as defined by equation 3.46. This final expression is used in the data processing to determine the reduced elevator deflection. The thrust moment arm $C_{m_{T_c}}$ is known, $\delta_{e_{meas}}$ is measured and the calculation for C_{m_δ} is explained in the subsection 3.4.5.

$$\delta_e^* = \delta_{e_{meas}} - \frac{C_{m_{T_c}}(T_{c_s} - T_c)}{C_{m_\delta}} \tag{3.46}$$

The thrust coefficient T_c is calculated with equation 3.47 [4], in which S is given and T_p, V_{TAS} and ρ are determined as explained in section 3.3. The standard thrust coefficient, T_{c_s} can be obtained with the same equation by using the standard thrust T_{p_s}, of which the calculation is done as with the actual thrust by using the standard fuel flow $\dot{m}_{f_s}$. This equation assumes that the thrust is independent of airspeed for constant throttle setting, which is valid for relatively low velocities as the velocities at which the aircraft in question operates.

$$T_c = \frac{2T_p}{\rho V_{TAS}^2 S} \tag{3.47}$$

3.4.2 Reduced elevator control force

The elevator control force is defined by equation 3.48 [4]. This force is a part of the measured data and can be reduced to standard values by converting and reducing the true airspeed to reduced equivalent airspeed as explained in the previous subsection resulting in equation 3.49.

$$F_e = \frac{d\delta_e}{ds_e}S_e\bar{c_e}\left(\frac{V_h}{V_{TAS}}\right)^2\left(\frac{C_{h_\delta}}{C_{m_\delta}}\frac{x_{cg} - x_{n_{free}}}{\bar{c}}\frac{W}{S} - \frac{1}{2}\rho V^2 C_{h_{\delta_t}}\left(\delta_{t_e} - \delta_{t_{e0}}\right)\right) \tag{3.48}$$

$$F_e^* = F_e\frac{W_s}{W} \tag{3.49}$$

3.4.3 Elevator effectiveness

To determine C_{m_δ}, firstly equation 3.41 is rewritten as equation 3.50 for equilibrium conditions. From this equation it can seen that a change in moment ΔC_m, created by the normal force C_N and the change in centre of gravity Δx_{cg}, must be overcome by a change in elevator deflection $\Delta\delta_e$. By applying a known Δx_{cg} and measuring the required $\Delta\delta_e$ the elevator effectiveness can be calculated with equation 3.51.

$$C_m = C_m|_{\delta_e=0} + C_{m_\delta}\delta_e = 0 \tag{3.50}$$

$$C_{m_\delta} = -\frac{1}{\Delta\delta_e}C_N\frac{\Delta x_{cg}}{\bar{c}} \tag{3.51}$$

C_N can be calculated as explained in section 3.3 and $\bar{c}$ is a known value. The change in C_N due to the changed elevator angle and the change in C_{m_δ} due to a change in the centre of gravity are both neglected in this equation.

3.4.4 Centre of gravity

The centre of gravity can be determined by taking all of the separate weights (empty weight, fuel weight and passengers+baggage) and their locations with respect to the front of the aircraft. The weight of each part is multiplied with the distance (in x-direction) to the nose of the aircraft, these moments are then summed and divided by the total weight. The result is the center of gravity x_{cg} where $x = 0$ is at the front of the aircraft.

3.4.5 Longitudinal stability

Taking the derivative of equation 3.41 with respect to the angle of attack α and rewriting gives the expression to determine the longitudinal stability C_{m_α} as given by equation 3.52. $\frac{d\delta_e}{d\alpha}$ can be determined by plotting the δ_e-α curve using the test data.

$$C_{m_\alpha} = -C_{m_\delta}\frac{d\delta_e}{d\alpha} \tag{3.52}$$

3.4.6 Results of second measurement series

This section presents the analytical results of a preselected measurement point. The input data corresponding to the selected measurement point are given in table 3.2 along with their values after the conversion to the desired units.

Table 3.2: The data corresponding to the measurement point, selected for the analytical results. In the first row, the first units correspond to the second row values and the second units correspond to the third row values. The second row gives the original data and the third gives the converted data.

h_p [ft,m]	V_c [kts,$\frac{m}{s}$]	α [$^\circ$,rad]	δ_e [$^\circ$,rad]	δ_{e_t} [$^\circ$,rad]	F_e [N]	$\dot{m}_{f_l}$ [$\frac{lbs}{hr}$,$\frac{kg}{s}$]	$\dot{m}_{f_r}$ [$\frac{lbs}{hr}$,$\frac{kg}{s}$]	F_{used} [lbs,kg]	T_m [$^\circ C$,K]
7090	161	4.8	-1	2.4	-1	437	481	606	7.2
2161.032	82.826	0.083776	-0.01745	0.04189	-1	0.055061	0.060605	274.877	280.35

The converted data can then be used for the reduction calculations. First the pressure p, the mach number M, the speed of sound a, the true airspeed V_{TAS}, the static air temperature T and air density ρ are calculated according to equations 3.53, 3.54, 3.56, 3.57 and 3.58, respectively.

These equations have already been explained in subsection 3.3.1. In each equation the known values of the measurement data as given in table 3.2, the known values of constants as defined in table 3.1 and the already calculated values are inserted. The latter also goes for the rest of the parameters of the calculations in this subsection, except for parameter values which are explicitly stated.

$$p = p_0\left(1+\frac{\lambda h_p}{T_0}\right)^{-\frac{g_0}{\lambda R}} = 101325\left(1+\frac{-0.0065*2161.032}{288}\right)^{-\frac{9.81}{-0.0065*287.05}} = 77900.453 \tag{3.53}$$

$$M = \sqrt{\frac{2}{\gamma-1}\left(\left(1+\frac{p_0}{p}\left(\left(1+\frac{\gamma-1}{2\gamma}\frac{\rho_0}{p_0}V_c^2\right)^{\frac{\gamma}{\gamma-1}}-1\right)\right)^{\frac{\gamma-1}{\gamma}}-1\right)} = \sqrt{\frac{2}{1.4-1}\left(\left(1+\frac{101325}{77900.453}\left(\left(1+\frac{1.4-1}{2*1.4}\frac{1.225}{101325}82.826^2\right)^{\frac{1.4}{1.4-1}}-1\right)\right)^{\frac{1.4-1}{1.4}}-1\right)} = 0.277 \tag{3.54}$$

$$T = \frac{T_m}{1+\frac{\gamma-1}{2}M^2} = \frac{280.35}{1+\frac{1.4-1}{2}0.277^2} = 276.113 \tag{3.55}$$

$$a = \sqrt{\gamma RT} = \sqrt{1.4*287.05*276.113} = 333.109 \tag{3.56}$$

$$V_{TAS} = Ma = 0.277*333.109 = 92.271 \tag{3.57}$$

$$\rho = \frac{p}{RT} = \frac{77900.453}{287.05*276.113} = 0.983 \tag{3.58}$$

For further calculations the weight of the aircraft is needed, which is calculated by subtracting the weight of the used fuel mass F_{used} from ramp weight W_r according to equation 3.59.

$$W = W_r - g_0 F_{used} = 61234.029 - 9.81*274.877 = 58537.486 \tag{3.59}$$

With the calculated weight W and density ρ the true airspeed is converted and reduced to the reduced equivalent airspeed by combining equations 3.43 and 3.44 into equation 3.60. The standard weight W_s is constant value defined as 60500 N.

$$\widetilde{V_e} = V_{TAS}\sqrt{\frac{\rho}{\rho_0}}\sqrt{\frac{W_s}{W}} = 92.271\sqrt{\frac{0.983}{1.225}}\sqrt{\frac{60500}{58537.486}} = 84.03 \tag{3.60}$$

The elevator control force can be reduced using equation 3.49 and its calculation is given by equation 3.61.

$$F_e^* = F_e\frac{W_s}{W} = -1\frac{60500}{58537.486} = -1.034 \tag{3.61}$$

The thrust coefficient and the standard thrust coefficient are necessary to calculate the reduced elevator deflection. These calculations are shown in equations 3.62 and 3.63. The thrust T_p and the standard thrust T_{p_s} were calculated by the program `thrust.exe` as explained in subsection 3.3.3 and were found to be 3867.58 N and 2736.42

respectively for this measurement point. T_{p_s} was calculated by using the standard fuel flow of 0.048 $\frac{kg}{s}$ for both engines instead of the actual fuel flow.

$$T_c = \frac{2T_p}{\rho V_{TAS}^2 S} = \frac{2 * 3867.58}{0.983 * 92.271^2 * 30} = 0.0308 \tag{3.62}$$

$$T_{c_s} = \frac{2T_{p_s}}{\rho V_{TAS}^2 S} = \frac{2 * 2736.42}{0.983 * 92.271^2 * 30} = 0.0218 \tag{3.63}$$

The elevator effectiveness is calculated with equation 3.51 using two adjacent measurement points. The change in elevator deflection $\Delta\delta_e$ was measured to be -0.00873 *rad*. The centres of gravity of the two measurement points are calculated as explained in section 3.4.4 and their difference was found to be -0.07764 *m*. The normal force coefficient C_N was calculated according to equation 3.25 and was equal to 0.466. C_{m_δ} is then defined by equation 3.64.

$$C_{m_\delta} = -\frac{1}{\Delta\delta_e} C_N \frac{\Delta x_{cg}}{\bar{c}} = -\frac{1}{-0.00873} 0.466 \frac{-0.07764}{2.0569} = -2.015 \tag{3.64}$$

The reduced elevator deflection is now calculated with equation 3.46. This is shown in equation 3.65. The thrust moment arm $C_{m_{T_c}}$ is known to be -0.0064.

$$\delta_e^* = \delta_{e_{meas}} - \frac{C_{m_{T_c}}(T_{c_s} - T_c)}{C_{m_\delta}} = -0.01745 - \frac{-0.0064(0.0218 - 0.0308)}{-2.015} = -0.0174 \tag{3.65}$$

The longitudinal stability, C_{m_α} is calculated as in equation 3.66. $\frac{d\delta_e}{d\alpha}$ is determined by setting up the $d\delta_e$-$d\alpha$ curve using all the measurement points and determining its slope, found to be -0.645.

$$C_{m_\alpha} = -C_{m_\delta} \frac{d\delta_e}{d\alpha} = -(-2.015) * (-0.645) = -1.3 \tag{3.66}$$

None of the produced results are unusual. All atmospheric parameters realistic values. Same goes for the reduced equivalent airspeed, the reduced control force and the reduced elevator deflection. In addition, the elevator effectiveness and longitudinal stability were also found to be realistic.

3.5 Assumptions of the analytical solution

For the analytical solution all the assumptions mentioned in chapter 2 apply. Moreover, two extra *secondary* assumptions were made in order to derive these equations:

- All force and moment coefficients behave linearly for small angles and small angle rates [4]. Extreme angles and angle rates are not realistic for a civilian aircraft and also not for this early design stage. Therefore, this assumption is considered to be a secondary assumption.
- The presence of a trim tab is neglected. This is a secondary assumption, because the deflection of the trim tab has a negligible effect on the forces along all three axes and, furthermore, the contribution to the pitching moment is negligible.

3.5.1 effect of assumptions on analytical results

The effect of the general assumptions and the analytical assumptions are small. The main assumptions that have small effect are that the aircraft is a rigid body, the aircraft deforms slightly during flight so will give slightly different aerodynamic properties, this may result in small deviations with reality. It was also assumed that there is no wind, depending on the flight conditions this can give big effects. The validation data was obtained in a flight with fairly low wind speeds so this assumptions should not give big deviations.

4. Numerical solution

This chapter gives an overview of the numerical model simulating the response of the aircraft. Section 4.8 presents the assumptions specific for the numerical model. Section 4.2 shows the outline for the simulation program.

4.1 State-space form of the equations of motion

The equations of motion 3.7 and 3.8 must be converted to state-space form given by equations 4.1 and 4.1. First, the equation is rewritten as 4.3. Then, rearranging terms and multiplying every term with the inverse of C_1, equation 4.3 is rewritten as equation 4.4. A comparison of equations 4.1 and 4.4 shows that state-space matrices A and B are defined by equations 4.5 and 4.6. Now the state and input vectors $\bar{x}$ and $\bar{u}$, the state matrix A and the input matrix B are determined.

Before applying the procedure explained above to equations 3.7 and 3.8, these equations can be written in a more convenient form. First, the differential operators D_c and D_b can be replaced with their expressions $\frac{\bar{c}}{V_0}\frac{d}{dt}$ and $\frac{b}{V_0}\frac{d}{dt}$ respectively. Next, the factors $\frac{\bar{c}}{V_0}$ and $\frac{b}{2V_0}$ can be relocated from the vectors to the matrices. Finally, $\hat{u}$ can be replaced with its expression $\frac{u}{V_0}$ and the factor $\frac{1}{V_0}$ can be relocated to the matrix. These operations result in the equations of motion 4.7 and 4.8. The next paragraph explains how equations 4.7 and 4.8 are converted to state-space by the procedure explained in the first paragraph of this section.

$$\dot{\bar{x}} = A\bar{x} + B\bar{u} \tag{4.1}$$

$$\bar{y} = C\bar{x} + D\bar{u} \tag{4.2}$$

$$C_1\dot{\bar{x}} + C_2\bar{x} + C_3\bar{u} = \bar{0} \tag{4.3}$$

$$\dot{\bar{x}} = -C_1^{-1}C_2\bar{x} - C_1^{-1}C_3\bar{u} \tag{4.4}$$

$$A = -C_1^{-1}C_2 \tag{4.5}$$

$$B = -C_1^{-1}C_3 \tag{4.6}$$

$$\begin{bmatrix} \frac{1}{V_0}(C_{X_U} - 2\mu_c\frac{\bar{c}}{V_0}\frac{d}{dt}) & C_{X_\alpha} & C_{Z_0} & \frac{\bar{c}}{V_0}C_{X_q} \\ \frac{C_{Z_u}}{V_0} & C_{Z_\alpha} + (C_{Z_{\dot{\alpha}}} - 2\mu_c)\frac{\bar{c}}{V_0}\frac{d}{dt} & -C_{X_0} & \frac{\bar{c}}{V_0}(C_{Z_q} + 2\mu_c) \\ 0 & 0 & -\frac{\bar{c}}{V_0}\frac{d}{dt} & \frac{\bar{c}}{V_0} \\ \frac{C_{m_u}}{V_0} & C_{m_\alpha} + C_{m_{\dot{\alpha}}}\frac{\bar{c}}{V_0}\frac{d}{dt} & 0 & \frac{\bar{c}}{V_0}(C_{m_q} - 2\mu_c K_Y^2\frac{\bar{c}}{V_0}\frac{d}{dt}) \end{bmatrix} \cdot \begin{bmatrix} u \\ \alpha \\ \theta \\ q \end{bmatrix} = \begin{bmatrix} -C_{X_{\delta_e}} \\ -C_{Z_{\delta_e}} \\ 0 \\ -C_{m_{\delta_e}} \end{bmatrix} \cdot \delta_e \tag{4.7}$$

$$\begin{bmatrix} C_{Y_\beta} + \left(C_{Y_{\dot{\beta}}} - 2\mu_b\right)\frac{b}{V_0}\frac{d}{dt} & C_L & \frac{b}{2V_0}C_{Y_p} & \frac{b}{2V_0}(C_{Y_r} - 4\mu_b) \\ 0 & -\frac{1}{2}\frac{b}{V_0}\frac{d}{dt} & \frac{b}{2V_0} & 0 \\ C_{\ell_\beta} & 0 & \frac{b}{2V_0}(C_{\ell_p} - 4\mu_b K_X^2\frac{b}{V_0}\frac{d}{dt}) & \frac{b}{2V_0}(C_{\ell_r} + 4\mu_b K_{XZ}\frac{b}{V_0}\frac{d}{dt}) \\ C_{n_\beta} + C_{n_{\dot{\beta}}}\frac{b}{V_0}\frac{d}{dt} & 0 & \frac{b}{2V_0}(C_{n_p} + 4\mu_b K_{XZ}\frac{b}{V_0}\frac{d}{dt}) & \frac{b}{2V_0}(C_{n_r} - 4\mu_b K_Z^2\frac{b}{V_0}\frac{d}{dt}) \end{bmatrix} \cdot \begin{bmatrix} \beta \\ \varphi \\ p \\ r \end{bmatrix} = \begin{bmatrix} -C_{Y_{\delta_a}} \\ 0 \\ -C_{l_{\delta_a}} \\ -C_{n_{\delta_a}} \end{bmatrix} \cdot \delta_a + \begin{bmatrix} -C_{Y_{\delta_r}} \\ 0 \\ -C_{l_{\delta_r}} \\ -C_{n_{\delta_r}} \end{bmatrix} \cdot \delta_r \tag{4.8}$$

To rewrite equation 4.7 in the form of equation 4.3 first the control input must be written as a vector. Next, the left handed matrix multiplication must be evaluated, of which the resulting vector can be separated in two new vectors, for convenience called vectors **a** and **b**. Vector **a** contains only the elements with time derivatives and **b** contains all the remaining terms. Finally, **a** can be rewritten as a multiplication of a matrix with vector $[\dot{u}\ \dot{\alpha}\ \dot{\theta}\ \dot{q}]^T$ and **b** as a multiplication of a matrix with with vector $[u\ \alpha\ \theta\ q]^T$. These operations lead to equation 4.9. Repeating the same operations for equation 4.8 results in equation 4.10.

$$\begin{bmatrix} -2\mu_c\frac{\bar{c}}{V_0} & 0 & 0 & 0 \\ 0 & \frac{\bar{c}}{V_0}(C_{Z_{\dot{\alpha}}} - 2\mu_c) & 0 & 0 \\ 0 & 0 & -\frac{\bar{c}}{V_0} & 0 \\ 0 & C_{m_{\dot{\alpha}}}\frac{\bar{c}}{V_0} & 0 & -2\mu_c K_Y^2\frac{\bar{c}^2}{V_0^2} \end{bmatrix} \cdot \begin{bmatrix} \dot{u} \\ \dot{\alpha} \\ \dot{\theta} \\ \dot{q} \end{bmatrix} + \begin{bmatrix} \frac{1}{V_0}C_{X_u} & C_{X_\alpha} & C_{Z_0} & \frac{\bar{c}}{V_0}C_{X_q} \\ \frac{1}{V_0}C_{Z_u} & C_{Z_\alpha} & -C_{X_0} & \frac{\bar{c}}{V_0}(C_{Z_q} + 2\mu_c) \\ 0 & 0 & 0 & \frac{\bar{c}}{V_0} \\ \frac{1}{V_0}C_{m_u} & C_{m_\alpha} & 0 & \frac{\bar{c}}{V_0}C_{m_q} \end{bmatrix} \cdot \begin{bmatrix} u \\ \alpha \\ \theta \\ q \end{bmatrix} + \begin{bmatrix} C_{X_{\delta_e}} \\ C_{Z_{\delta_e}} \\ 0 \\ C_{m_{\delta_e}} \end{bmatrix} \cdot [\delta_e] = \begin{bmatrix} 0 \\ 0 \\ 0 \\ 0 \end{bmatrix} \tag{4.9}$$

$$\begin{bmatrix} \frac{b}{V_0}(C_{Y_{\dot\beta}}-2\mu_b) & 0 & 0 & 0 \\ 0 & -\frac{1}{2}\frac{b}{V_0} & 0 & 0 \\ 0 & 0 & -2\mu_b K_X^2 \frac{b^2}{V_0^2} & 2\mu_b K_{XZ}\frac{b^2}{V_0^2} \\ \frac{b}{V_0}C_{n_{\dot\beta}} & 0 & -2\mu_b K_{XZ}\frac{b^2}{V_0^2} & -2\mu_b K_Z^2\frac{b^2}{V_0^2} \end{bmatrix} \cdot \begin{bmatrix} \dot\beta \\ \dot\phi \\ \dot p \\ \dot r \end{bmatrix} + \begin{bmatrix} C_{Y_\beta} & C_L & \frac{b}{2V_0}C_{Y_p} & \frac{c}{2V_0}(C_{Y_r}-4\mu_b) \\ 0 & 0 & \frac{b}{2V_0} & 0 \\ C_{\ell_\beta} & 0 & \frac{b}{2V_0}C_{\ell_p} & \frac{b}{2V_0}C_{\ell_r} \\ C_{n_\beta} & 0 & \frac{b}{2V_0}C_{n_p} & \frac{b}{2V_0}C_{n_r} \end{bmatrix} \cdot \begin{bmatrix} \beta \\ \phi \\ p \\ r \end{bmatrix} + \begin{bmatrix} C_{Y_{\delta\alpha}} & C_{Y_{\delta_r}} \\ 0 & 0 \\ C_{l_{\delta\alpha}} & C_{l_{\delta_r}} \\ C_{n_{\delta\alpha}} & C_{n_{\delta_r}} \end{bmatrix} \cdot \begin{bmatrix} \delta_\alpha \\ \delta_r \end{bmatrix} = \begin{bmatrix} 0 \\ 0 \\ 0 \\ 0 \end{bmatrix} \quad (4.10)$$

From equation 4.9 the expressions for $\bar{x}$, $\bar{u}$, C_1, C_2 and C_3 for symmetric flight can be stated as in equations 4.11 up to 4.15 and for asymmetric flight can be stated as in equations 4.16 up to 4.20.

$$\bar{x_s} = [u \quad \alpha \quad \theta \quad q]^T \quad (4.11) \qquad \bar{u_s} = [\delta_e] \quad (4.12)$$

$$C_{1_s} = \begin{bmatrix} -2\mu_c\frac{\bar c}{V_0^2} & 0 & 0 & 0 \\ 0 & \frac{\bar c}{V_0}(C_{Z_\alpha}-2\mu_c) & 0 & 0 \\ 0 & 0 & -\frac{\bar c}{V_0} & 0 \\ 0 & C_{m_{\dot\alpha}}\frac{\bar c}{V_0} & 0 & -2\mu_c K_Y^2\frac{\bar c^2}{V_0^2} \end{bmatrix} \quad (4.13)$$

$$C_{2_s} = \begin{bmatrix} \frac{1}{V_0}C_{X_u} & C_{X_\alpha} & C_{Z_0} & \frac{\bar c}{V_0}C_{X_q} \\ \frac{1}{V_0}C_{Z_u} & C_{Z_\alpha} & -C_{X_0} & \frac{\bar c}{V_0}(C_{Z_q}+2\mu_c) \\ 0 & 0 & 0 & \frac{\bar c}{V_0} \\ \frac{1}{V_0}C_{m_u} & C_{m_\alpha} & 0 & \frac{\bar c}{V_0}C_{m_q} \end{bmatrix} \quad (4.14) \qquad C_{3_s} = \begin{bmatrix} C_{X_{\delta_e}} \\ C_{Z_{\delta_e}} \\ 0 \\ C_{m_{\delta_e}} \end{bmatrix} \quad (4.15)$$

$$\bar{x_a} = [\beta \quad \phi \quad p \quad r]^T \quad (4.16) \qquad \bar{u_a} = [\delta_a \quad \delta_r]^T \quad (4.17)$$

$$C_{1_a} = \begin{bmatrix} \frac{b}{V_0}(C_{Y_{\dot\beta}}-2\mu_b) & 0 & 0 & 0 \\ 0 & -\frac{1}{2}\frac{b}{V_0} & 0 & 0 \\ 0 & 0 & -2\mu_b K_X^2\frac{b^2}{V_0^2} & 2\mu_b K_{XZ}\frac{b^2}{V_0^2} \\ \frac{b}{V_0}C_{n_{\dot\beta}} & 0 & 2\mu_b K_{XZ}\frac{b^2}{V_0^2} & -2\mu_b K_Z^2\frac{b^2}{V_0^2} \end{bmatrix} \quad (4.18)$$

$$C_{2_a} = \begin{bmatrix} C_{Y_\beta} & C_L & \frac{b}{2V_0}C_{Y_p} & \frac{b}{2V_0}(C_{Y_r}-4\mu_b) \\ 0 & 0 & \frac{b}{2V_0} & 0 \\ C_{\ell_\beta} & 0 & \frac{b}{2V_0}C_{\ell_p} & \frac{b}{2V_0}C_{\ell_r} \\ C_{n_\beta} & 0 & \frac{b}{2V_0}C_{n_p} & \frac{b}{2V_0}C_{n_r} \end{bmatrix} \quad (4.19) \qquad C_{3_a} = \begin{bmatrix} C_{Y_{\delta\alpha}} & C_{Y_{\delta_r}} \\ 0 & 0 \\ C_{\ell_{\delta\alpha}} & C_{\ell_{\delta_r}} \\ C_{n_{\delta\alpha}} & C_{n_{\delta_r}} \end{bmatrix} \quad (4.20)$$

By substituting the expressions for C_1, C_2 and C_3 in equations 4.5 and 4.6 the state matrix A and input matrix B can be determined. resulting in equations 4.21 and 4.23 for symmetric flight and 4.22 and 4.24 for asymmetric flight.

$$A_s = \begin{bmatrix} \frac{V_0 C_{X_u}}{2\mu_c\bar c} & \frac{V_0^2 C_{X_\alpha}}{2\bar c\mu_c} & \frac{V_0^2 C_{Z_0}}{2\bar c\mu_c} & \frac{V_0 C_{X_q}}{2\mu_c} \\ \frac{C_{Z_u}}{\bar c(2\mu_c - C_{Z_{\dot\alpha}})} & \frac{V_0 C_{Z_\alpha}}{\bar c(2\mu_c - C_{Z_{\dot\alpha}})} & \frac{V_0 C_{X_0}}{\bar c(C_{Z_{\dot\alpha}} - 2\mu_c)} & \frac{V_0}{\bar c}\frac{2\mu_c + C_{Z_q}}{2\mu_c - C_{Z_{\dot\alpha}}} \\ 0 & 0 & 0 & 1 \\ \frac{V_0}{2\mu_c\bar c^2 K_Y^2}(C_{m_u} + \frac{C_{m_{\dot\alpha}}C_{Z_u}}{2\mu_c - C_{Z_{\dot\alpha}}}) & \frac{V_0^2}{2\mu_c\bar c^2 K_Y^2}(C_{m_\alpha} + \frac{C_{m_{\dot\alpha}}C_{Z_\alpha}}{2\mu_c - C_{Z_{\dot\alpha}}}) & \frac{V_0^2 C_{m_{\dot\alpha}}C_{X_0}}{2\mu_c\bar c^2 K_Y^2(C_{Z_{\dot\alpha}} - 2\mu_c)} & \frac{V_0}{2\mu_c\bar c K_Y^2}(\frac{C_{Z_q}+2\mu_c}{2\mu_c - C_{Z_{\dot\alpha}}} + C_{m_q}) \end{bmatrix} \quad (4.21)$$

$$A_a = \begin{bmatrix} \frac{V_0}{b}\frac{C_{Y_\beta}}{2\mu_b} & \frac{V_0}{b}\frac{C_L}{2\mu_b} & \frac{V_0}{b}\frac{C_{Y_p}}{2\mu_b} & \frac{V_0}{b}\frac{C_{Y_r}}{2\mu_b} \\ 0 & 0 & \frac{2V_0}{b} & 0 \\ \frac{2V_0^2}{b^2}\frac{C_{\ell_\beta}K_Z^2+C_{n_\beta}K_{XZ}}{4\mu_b(K_X^2K_Z^2-K_{XZ}^2)} & 0 & \frac{2V}{b}\frac{V}{b}\frac{C_{\ell_p}K_Z^2+C_{n_p}K_{XZ}}{4\mu_b(K_X^2K_Z^2-K_{XZ}^2)} & \frac{2V_0^2}{b^2}\frac{C_{\ell_r}K_Z^2+C_{n_r}K_{XZ}}{4\mu_b(K_X^2K_Z^2-K_{XZ}^2)} \\ \frac{2V_0^2}{b^2}\frac{C_{\ell_\beta}K_{XZ}+C_{n_\beta}K_X^2}{4\mu_b(K_X^2K_Z^2-K_{XZ}^2)} & 0 & \frac{2V_0^2}{b^2}\frac{C_{\ell_p}K_{XZ}+C_{n_p}K_X^2}{4\mu_b(K_X^2K_Z^2-K_{XZ}^2)} & \frac{2V_0^2}{b^2}\frac{C_{\ell_r}K_{XZ}+C_{n_r}K_X^2}{4\mu_b(K_X^2K_Z^2-K_{XZ}^2)} \end{bmatrix} \tag{4.22}$$

$$B_s = \begin{bmatrix} \frac{V_0^2 C_{X_{\delta_e}}}{2\mu_c \bar{c}} \\ \frac{V_0 C_{X_{\delta_e}}}{\bar{c}(2\mu_c - C_{Z_{\dot\alpha}})} \\ 0 \\ \frac{V_0^2}{2\mu_c \bar{c}^2 K_Y^2}\left(\frac{C_{m_{\dot\alpha}}C_{Z_{\delta_e}}}{2\mu_c - C_{Z_{\dot\alpha}}} + C_{m_{\delta_e}}\right) \end{bmatrix} \tag{4.23}$$

$$B_a = \begin{bmatrix} 0 & \frac{V_0}{b}\frac{C_{Y_{\delta_r}}}{2\mu_b} \\ 0 & 0 \\ \frac{2V_0^2}{b^2}\frac{C_{\ell_{\delta_\alpha}}K_Z^2+C_{n_{\delta_\alpha}}K_{XZ}}{4\mu_b(K_X^2K_Z^2-K_{XZ}^2)} & \frac{2V_0^2}{b^2}\frac{C_{\ell_{\delta_r}}K_Z^2+C_{n_{\delta_r}}K_{XZ}}{4\mu_b(K_X^2K_Z^2-K_{XZ}^2)} \\ \frac{2V_0^2}{b^2}\frac{C_{\ell_{\delta_\alpha}}K_{XZ}+C_{n_{\delta_\alpha}}K_X^2}{4\mu_b(K_X^2K_Z^2-K_{XZ}^2)} & \frac{2V_0^2}{b^2}\frac{C_{\ell_{\delta_r}}K_{XZ}+C_{n_{\delta_r}}K_X^2}{4\mu_b(K_X^2K_Z^2-K_{XZ}^2)} \end{bmatrix} \tag{4.24}$$

The output matrix C depends on the desired outputs. For both the symmetric as well as the asymmetric flight condition most of the desired outputs are also present in the state vector x. The only exception is the airspeed V. However, to determine V the deviation from the initial velocity u is needed which is also in the state vectors. Therefore, it can be concluded that C should be an unit matrix for both flight conditions. Since the elements of the input vector $\bar{u}$ are not needed for the outputs for both the symmetric as well as the asymmetric case, the feedback matrix D becomes a zero matrix for both flight conditions. The output and feedback matrices C and D for both flight conditions are given by equations 4.25, 4.26 and 4.27.

Solving this state-space system gives the dynamic response of the aircraft: the deviation of the initial velocity u, the angle of attack α, the pitching angle θ, the angle of side slip β, the angle of roll ϕ, the pitching rate q, the roll rate p and the yaw rate r w.r.t. time. To solve the state-space system the MATLAB Control System Toolbox is used. The responses to arbitrary, step, pulse and zero input signals can then be easily extracted and plotted. In order to get the plot of the true airspeed V, one simply needs to add the initial velocity V_0 to the deviation of the initial velocity u ($V(t) = V_o + u(t)$).

$$C_s = C_a = \begin{bmatrix} 1 & 0 & 0 & 0 \\ 0 & 1 & 0 & 0 \\ 0 & 0 & 1 & 0 \\ 0 & 0 & 0 & 1 \end{bmatrix} \tag{4.25}$$

$$D_s = \begin{bmatrix} 0 \\ 0 \\ 0 \\ 0 \end{bmatrix} \tag{4.26}$$

$$D_a = \begin{bmatrix} 0 & 0 \\ 0 & 0 \\ 0 & 0 \\ 0 & 0 \end{bmatrix} \tag{4.27}$$

4.2 Flowchart of simulation program

The flowchart in figure 4.1 shows the overview of the simulation program. Firstly, all data is loaded from the provided `Cit_par.mat` file, this may (for the improved model) include the output data from the first and second measurement series. After this the C1,C2 and C3 for both the symmetrical case and the asymmetric case is calculated. Next the A, B, C and D are determined, from that the eigenvalues, the damping half-time and the period are calculated for verification purposes. Finally the response to a given input is plotted.

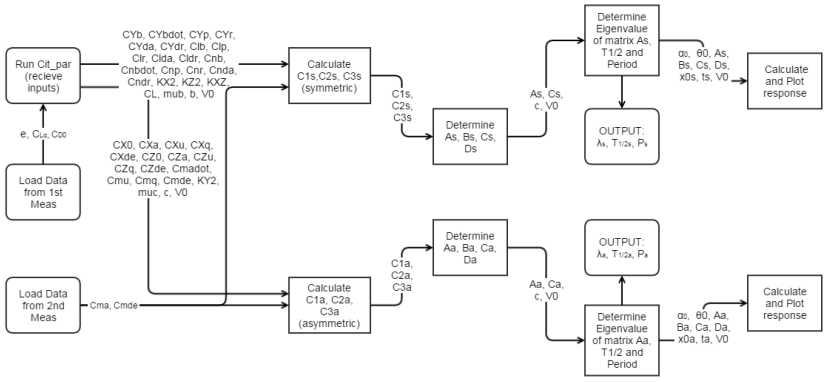

Figure 4.1: flowchart for the simulation program

4.3 Results simulation program

The figure 4.2a and figure 4.2b below are the results coming from a step input of minus one degree of the elevator, and a initial state for the roll angle of 15°.

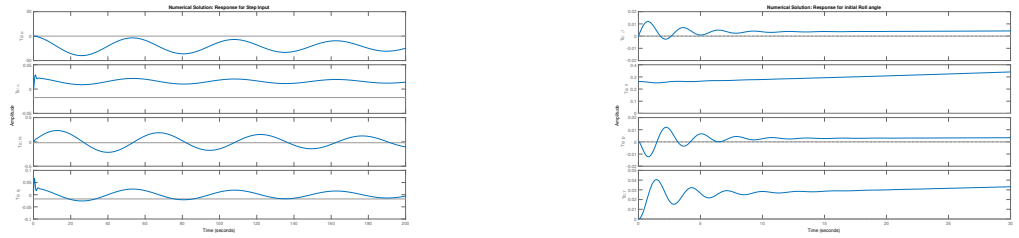

(a) The step response for the elevator deflection

(b) The response to an initial state of the roll angle

Figure 4.2

The main shape of the response to a step input seems to be correct, there are no extreme errors to be found in the response. However, there are still some things that are incorrect. For instance, the airspeed has an extreme amplitude of almost 50, which is around half the initial true airspeed. This cannot be correct, the error is expected to be a result of inconsistent use of units. Besides that, the jump at the start of the graph in the angle of attack seems correct, as an effect of the step input of the elevator deflection. The same holds for the pitching rate, which shows a jump at the start of the graphy due to the sudden impact of the step input, and after that it damps. The pitch itself also shows logical results.

For the response to the initial roll angle is increasing further as can be seen in figure 4.2b. This makes sense due to the unstable characteristics of the manoeuvre. The roll rate also makes sense, since it damps to a positive value which slightly increases after that.

4.4 Flowchart of first measurement series program

A flowchart for the program that will do the data processing of measurement series 1 can be seen in figure 4.3.

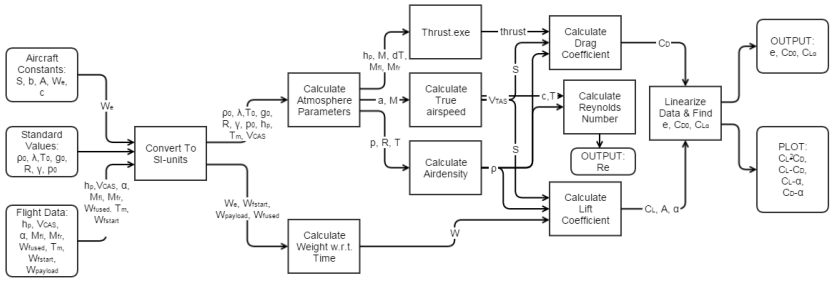

Figure 4.3: flowchart for the first measurement series program

The measurement data is not provided in SI units, so these are converted first. The method for the rest of the calculations in this program can be found in section 3.3. Firstly the atmosphere parameters are calculated for the respective altitude, afterwards the thrust, the true airspeed, the air density and the weight at the time of measurement are calculated. Now the C_L and C_D can be calculated which are then used for all of the needed plots. Besides these plots the program also calculates the Reynolds number (to be able to compare the data to other cases). Finally the Oswald factor, zero-lift-drag-coefficient and the lift slope are calculated for the improvement of the simulation program.

4.5 Results first measurement series

The testdata was obtained in the 4th test flight of 6-3-2015. The result of the first measurement series with this data consists of 4 plots, the Oswald factor, the zero lift drag-coefficient and lift slope. The plots are shown in figure 4.4.

The calculated Oswald factor is 0.8124, this result is reasonable as most aircraft have an Oswald factor between 0.7 and 0.85 [6]. The zero lift drag-coefficient was calculated to be 0.025, the zero lift drag-coefficient is generally between 0.01 and 0.04 [3] so the value is within this range. The lift slope C_{L_α} was calculated to be 4.4327 per rad. For thin airfoils the lift slope is $2\pi = 6.28$ per rad, the calculated value is thus close to the 2D thin airfoil lift slope, the value is lower due to 3D effects.

Top left plot of figure 4.4 shows that the measured points are almost in a straight line. They are supposed to be linear due to equation 3.26, so the measurement points are in sync with the theory. The bottom left plot is perfectly linear, this is also as expected as the measurement points were taken when the aircraft was not stalling (or near to stall), this means that the $C_L - \alpha$ curve is in its linear part. The top right graph is (due to again equation 3.26) expected to look like a square root function. The points do form this distinct shape in the graph. The bottom right

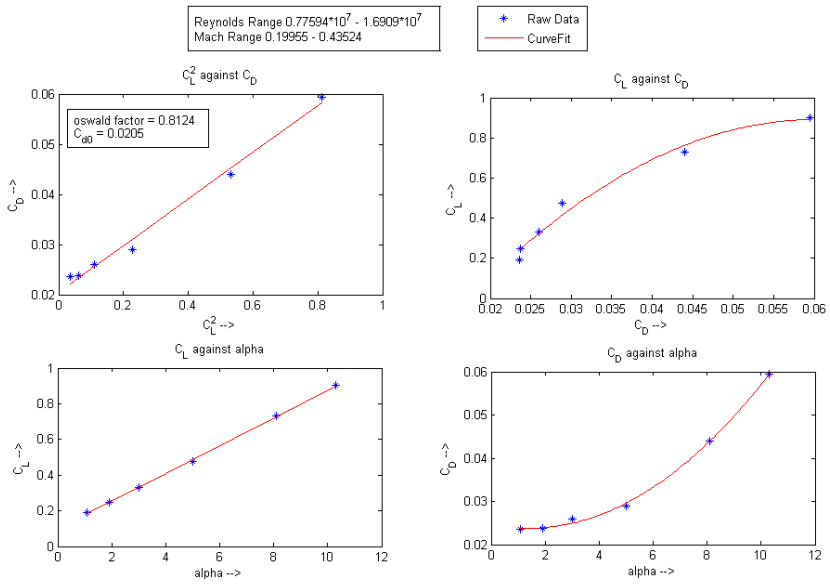

Figure 4.4: Reference frames projected on front view of aircraft

curve is shaped like a parabola, since 3.26 uses $C_L{}^2$ and C_L depends on alpha this is again expected since C_D thus depends on α^2.

4.6 Flowchart of second measurement series program

The flowchart of the second measurement series is presented in figure 4.5. First, the measured data is converted into SI units. The program then calculates the standard atmosphere parameters at the altitude of the measurements, the instantaneous weight and center of gravity. Then, the thrust, true airspeed and the air density are calculated. Following this, the standard and actual thrust coefficient, the normal force coefficient and the elevator effectiveness are calculated. Finally the reduced elevator control force, the reduced elevator deflection and the reduced equivalent airspeed are calculated. The final step in the program is to plot the reduced elevator trim curve and the reduced control force curve.

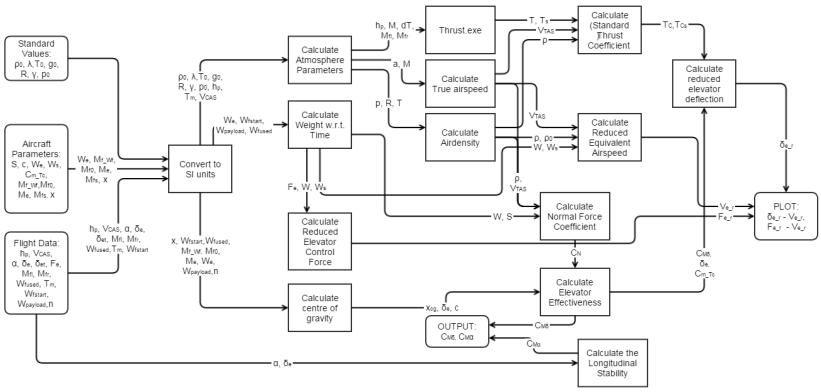

Figure 4.5: flowchart for the second measurement series program

4.7 Results second measurement series

From the second measurement series program the results are not only used to investigate the static stability of the aircraft, but also to verify the program. The results of this test is given by table 4.1 and by figures 4.6 and 4.7. Table 4.1 gives the elevator effectiveness and the longitudinal stability and also the values of the reduced equivalent airspeed, reduced control force curve and reduced elevator deflection of the measurement point that was used in subsection 3.4.6. Figures 4.6 and 4.7 give the elevator trim curve and the elevator control force curve, respectively.

In the table 4.1 it can be seen that the data processing program gives realistic values as outputs just like the analytical solution: the calculated stability coefficients and the calculated reduced parameters are within the range which is physically possible for an aircraft. For the verification of these numerical results with the analytical results of subsection 3.4.6, the reader is referred to subsection 5.2.2.

Table 4.1: The results obtained from the data processing program of the second measurement series to investigate static stability and to perform program verification.

C_{m_α} [-]	C_{m_δ} [-]	$\widetilde{V_e}$ $[\frac{m}{s}]$	F_e^* $[N]$	δ_e^* $[rad]$
-1.285	-1.993	84.019	-1.034	-0.0174

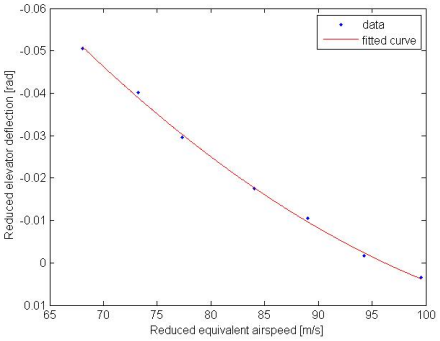

Figure 4.6: The trim curve in clean configuration forwhich the flap deflection and the landing gear positionfor coefficient are always zero ($\delta_f = 0$ and $C_{m_{lg}}|_{lgdown} = 0$).coefficient are always zero ($\delta_f = 0$ and $C_{m_{lg}}|_{lgdown} = 0$). The fuel flow range for these data points was: $0.053 \leq$The fuel flow range for these data points was: $0.053 \leq \dot{m}_f[kg/s] \leq 0.062$ $\dot{m}_f[kg/s] \leq 0.062$

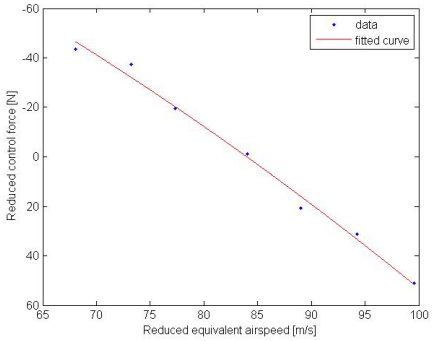

Figure 4.7: The control force curve in clean configuration

Also the trim and control force curve have the expected outcome: the trim curve has a logarithmic shape and the control force curve an exponential shape. Considering the how close the data points are located to the fitted curve, one can conclude that these measurements are sufficiently accurate to use them for the stability analysis.

In table 4.1 it can be seen that C_{m_α} is negative. Which means that the aircraft has stick fixed static longitudinal stability. In figure 4.6 it can be seen that $\frac{\delta_e^*}{\widetilde{V_e}}$ is positive for all air speeds, which automatically means that the prototype has also trim stability. Both characteristics make the aircraft safer to fly during stick fixed conditions.

From figure 4.7 it can be seen that the slope of the reduced stick force with respect to the reduced equivalent airspeed is positive ($\frac{dF_e^*}{d\widetilde{V_e}} > 0$) at the trim speed (the speed at the force is zero). This means that the aircraft has control force stability at the trim speed. Due to this characteristic the prototype is more pleasant and safer to fly for the pilot. This characteristic is also an indication the aircraft is static longitudinally stable during stick free conditions. To be certain that the aircraft really has stick free static longitudinal stability, more information about the aircraft configuration and flight conditions is needed as explained in chapter 10 of [4].

4.8 Assumptions of the numerical solution

To get from the analytical to the numerical solution it is assumed that the state-space form can be used. The state-space form can only be used for linear time-invariant systems, which means that the elements of the state-space matrices must be all constant. However, the elements of those state-space matrices depend on the slopes of the aerodynamic force and moment coefficient of the aircraft and the relative densities (μ_b and μ_c), which again depend on the aircraft mass and air density. The aerodynamic coefficient slopes, the aircraft mass and air density are not constant during real flight. Therefore, it is not valid to use the state-space form for the equations of motion of real flight.

However, the simulation is made to predict the aircraft behaviour for short time intervals, thus the aircraft mass will be almost constant during that interval. In that time interval the aircraft is not meant to change altitude significantly and thus the air density will be nearly constant as well. The aerodynamic coefficient slopes are all nearly invariable for small deviations of u, α, θ, q, β, ϕ, p and r. The simulation tool is indeed meant to be used for only small deviations of all the aforementioned parameters and thus the elements of the state-space matrices will be nearly constant and the state-space form is allowed to be used. The assumption that the state-space form can be used will have small impact on the results of the simulation tool and thus this a *secondary assumption*.

4.8.1 Effects of assumptions on numerical results

The effects that were stated in section 3.5.1 are also effects on the numerical solution, the new assumption that values stay constant within a motion has a small effect on the solution, many values change during a flight but since

the results that are plotted are generally over a short period of time the neglecting of the changes is valid.

5. Verification

This chapter explains the verification procedure applied to the simulation. Unit tests and system tests for the three modules of the simulation are explained. Each system test is followed by a subsequent discussion about found discrepancies and how they are related to the assumptions used to implement the numerical solution.

5.1 First measurement series

This section presents the unit and system tests that were ran on the calculations that process the data of the first measurement series of the flight test.

5.1.1 Unit tests of first measurement series

This section explains the unit tests ran on the calculations of the first measurement series. Inputs and outputs are not given for all units, since some of them are single and simple linear expressions. For more complicated functions, inputs and outputs are given.

Atmospheric parameters

The unit `AtmosphereParameters` is relatively extensive. Therefore, the inputs and outputs used to verify this unit are given in table 5.1. They are an exact match to the analytical expressions, except for rounding error due to a difference in significant number count. Singularity checks with zero and negative inputs were also ran to check that the module raises errors when unrealistic values are input.

Table 5.1: Comparison of analytical and numerical results for the unit `AtmosphereParameters`. All results are rounded to integers.

INPUT	
Variable	Input value
P_0	101325
ρ_0	1.2250
λ	-0.0065
h_p	[2000,2500,3000]
T_0	288
T_m	[280,285,290]
g_0	9.81
R	287.05
γ	1.4
V_{CAS}	[80,100,120

OUTPUT (converted & rounded to integers)		
Variable	Analytical	Numerical
p	[79478,74662,70086]	[79478,74662,70086]
M*1000	[265,341,421]	[264,341,421]
T	[276,279,280]	[276,279,280]
a	[333,335,335]	[333,335,335]
dT*100	[112,677,1156]	[112,677,1156]

Execution of `thrust.exe`

Since the `thrust.exe` program was already verified and validated by the manufacturer, the output of this program is not tested fully. The `ThrustExecution` function is tested for displaying a correct output format, this is the case if a correct input format and realistic input values are provided. The output values are also tested to be realistic, this is done by comparing the total thrust to the total weight. The glide ratio W/thrust should be between 5 and 25 [1]. This is tested with data from a real flight and aircraft, the glide ratio for this data was between 9 and 19 so it is realistic.

Small units of first measurement series

This section documents the verification of the units too small to warrant a separate section. They have been checked as thoroughly as the other functions but explaining each of them would be redundant as each unit was verified in a similar manner.

- **Air density** The `AirDensity` function is tested for realistic input values and unrealistic cases where the function should return an error.
- **Drag coefficient** The `CD` function is verified with a realistic value test. Error raising was checked for the cases when the density, speed, wing area or the thrust are smaller than (or equal to) zero.
- **Lift coefficient** The `CL` function is verified for realistic values and for singularities. Error raising was checked for cases when density, speed, wing area or thrust are smaller than (or equal to) zero.
- **True airspeed** The `VTAS` function correctly multiplies M and a. Error raising was tested for negative input values.
- **Instantaneous weight** It is verified that the `WeightAtTime` function properly subtracts the `fuelUsed` from the `rampweight`. Error raising was tested for the case where output is negative and for the case where more fuel is used than the start fuel.

5.1.2 System test of first measurement series

In table 5.2 the results of the system test of the first measurement series calculations are presented. The errors are very small and due to the difference between significant figures used in analytical and numerical computations. Therefore the system is considered fully verified.

Table 5.2: System test results of the first measurement series.

Variable	Analytical value	Numerical value	Unit	difference (in %)
p	78049	78049	Pa	0.0
M	0.433	0.435	$-$	4
T	276.96	276.86	K	0.04
a	334.62	333.55	$\frac{m}{s}$	0.3
dT	2.91	2.8081	K	4
V_{tas}	145.44	145.18	$\frac{m}{s}$	0.2
ρ	0.9817	0.9821	$\frac{kg}{m}$	0.04
W	$6.1058 \cdot 10^4$	$6.1059 \cdot 10^4$	kg	$<$0.01
c_D	0.024	0.0236	$-$	2
c_L	0.196	0.1967	$-$	4
Re	$1.6928 \cdot 10^7$	$1.6909 \cdot 10^7$	$-$	0.11

5.2 Second measurement series

This section presents the unit and system tests that were ran on the calculations that process the data of the second measurement series of the flight test.

5.2.1 Unit tests of second measurement series

This section elaborates on the unit tests that were ran on the individual units of the calculations for the second measurement series. Some units are single linear expressions, for which inputs and outputs are not given. For relatively extensive units, they are given.

Center of gravity

The unit calculating the center of gravity was compared to an analytical calculation. Two fuel load cases have to be given to the program for calculating the change in center of gravity. The following inputs were used:

- Fuel weight at the start is $13000N$.
- Fuel used at state time 1 is $6000N$, fuel used at state 2 is $5000N$.
- $\frac{dM_{fuel}}{dW_{fuel}}$ is $7.2456m$.
- Empty fuel moment arm M_{fuel_0} (result of the regression of fuel moment tables) is $111.8Nm$.
- Aircraft empty weight moment is $302600.488Nm$.
- Aircraft empty weight is $40804.1N$.
- Payload consists of 9 persons of $800N$ weight on board.
- Locations of pilots, test coordinator, first row, second row, third row passengers w.r.t. aircraft nose along the x-axis are $1m, 3m, 5m, 7m, 9m$, respectively.

The program outputs for the first state a center of gravity of $7.1091m$ and for the second state $7.1245m$, in exact agreement with the analytical solution.

SI conversion unit

The conversion-to-SI unit was tested with inputs and the resulting outputs are given in table 5.3. The outputs are in full agreement with the results of the analytical solution.

Table 5.3: The inputs and outputs of the unit test of the conversion-to-SI program block.

Converted variable	Original value with unit	Converted value with unit
h_p	$1ft$	$0.3048m$
V_c	$1kts$	$0.5144m/s$
α	$180°$	$3.1416rad$
δ_e	$180°$	$3.1416rad$
M_{fl}	$1000lbs/hr$	$0.1260kg/s$
M_{fr}	$1000lbs/hr$	$0.1260kg/s$
$W_{F_{USED}}$	$100lbs$	$45.3592kg$
T_m	$1°C$	$274.1500K$
$W_{F_{START}}$	$100lbs$	$45.3592kg$
W_{empty}	$100lbs$	$45.3592kg$
$x-location$	$100inches$	$2.5400m$
$\frac{dM_{fuel}}{dW_{fuel}}$	$100inches$	$2.54m$
M_{fuel_0}	$100inch-lbs$	$1.1521Nm$
M_{empty}	$100inch-pounds$	$1.1521Nm$

Small unit tests for second measurement Series
This section covers unit tests for the second measurement series that were too small to warrant a separate discussion.

- **Atmospheric parameters** The unit that calculates the atmospheric parameters is identical to the one used in the calculations for the first measurement series. This unit was already verified in section 5.1.1.
- **Air density** The identical unit calculating air density was already verified for the first measurement series. This is documented in section 5.1.1.
- **True airspeed** The identical unit calculating true airspeed was already verified for the first measurement series. This is documented in section 5.1.1.
- **Aircraft weight** Output was verified for realistic inputs. Error raising was tested for cases where weight is less than (or equal to) zero.
- **Normal force coefficient** The `normal_force_coefficient` function is verified for realistic values and for singularities. Error raising was checked for cases when density, speed, wing area or thrust are smaller than (or equal to) zero.
- **Slope of trim curve** The output slope for a few input point was verified for realistic and singular values.
- **Longitudinal stability** The output C_{M_α} was verified for realistic inputs.
- **Elevator effectiveness** Output was verified for realistic inputs. Error raising checks were performed for negative or zero MAC input and zero change in elevator deflection.
- `Thrust` The unit executing `thrust.exe` was already verified for the first measurement series, as documented in section 5.1.1.
- **Reduced Equivalent airspeed** Output was verified for realistic inputs. Error raising was tested for negative/zero weight and sea level air density.
- **Thrust coefficient** The output was verified with realistic inputs. Error raising was tested for cases where denominator is zero.
- **Reduced equivalent elevator deflection** Output was verified for realistic inputs. Error raising was checked for division by zero case.
- **Reduced elevator control force** Output was verified for realistic values. Singularity checks not necessary as the instantaneous weight calculation unit already check for less than (or equal to) zero aircraft weight.

5.2.2 System test of second measurement series

The outputs of the data processing program of the second measurement series are C_{m_δ} and C_{m_α} and also F_e^*, $\widetilde{V_e}$ and δ_e^* for 7 measurement points. The analytically determined C_{m_δ} and C_{m_α} are given in subsection 3.4.6 and by comparison with the program results in section 4.7 it is found that the numerically calculated C_{m_δ} and C_{m_α} differ from the analytically calculated values with 1.1% and 1.2% respectively. These small differences arise from the difference in significant numbers used for the analytical and numerical calculations.

During the analytical calculations F_e^*, $\widetilde{V_e}$ and δ_e^* were only determined for 1 of the 7 measurement points. Performing the system test for only 1 measurement is sufficient, since the calculations are exactly the same for every point. It is found that for this point, the numerically calculated F_e^* and $\widetilde{V_e}$ differ from the analytically calculated values by 3.4% and 0.013% respectively. These differences also arise from the difference in significant numbers used for the analytical and numerical calculations. Regarding δ_e^* no discrepancies are found.

All identified discrepancies are due to rounding errors, as there are is no difference between the used calculations from a mathematical perspective. The calculations of the second measurement series are considered verified.

5.3 Aircraft dynamic response model

Using the design parameters of the prototype aircraft the preliminary model can be verified by means of unit and system tests. Plots are made of the prediction of the preliminary model regarding the response to certain inputs and disturbances to investigate the plausibility of the prediction.

5.3.1 Unit tests of dynamic response model

It is sufficient, for the dynamic response model, to compare the eigenvalues of the state matrices to the eigenvalues of the state-space matrix from of the symmetrical/asymmetrical equations of motion of the analytical solution. Other unit blocks of the dynamic response model are depending on matrix transformations, transformation from state-space to system and the system response to disturbance and state vector. These blocks are assumed to be correct since they are standard Matlab functions. The unit blocks were checked for implementation

A convenient way to compare the numerical and analytical solution is to compare the eigenvalues of matrices A_s and A_s as in equation 3.9 and 3.10 respectively. Using Matlab the eigenvalues are easily calculated in a numerical manner. On the other hand the eigenvalues are calculated analytically which can be seen in section 3.2.1. The eigenvalues resulting from both solutions can be seen in table 5.4

As can be seen in table 5.4 the discrepancy's between the eigenvalues are quite large. This is due to the wrong calculation of the eigenvalues in the numerical model. In the numerical model the eigenvalues are calculated using the standard Matlab function. This function uses a identity matrix of the same size, multiplies that with λ, subtracts this identity matrix form the state space matrix and then equates the determinant to zero. In the analytical solution the identity matrix is not used, but D_c and D_b are replaced with λ_b and λ_c respectively. This is is a fundamental

Eigenmotion	Short period		Phugoid		Aperiodic roll	Dutch Roll		Spiral
Analytical	$-0.0279 \pm 0.0433i$		$-0.000141 \pm 0.00268i$		-0.676	$-0.0579 \pm 0.339i$		0.00164
Numerical	$-0.00231 \pm 0.104i$		$-0.00316 \pm 0.104i$		-0.215	$-0.215 \pm 1.92i$		0.0095
Error	1,107%	140%	2,141%	3,781 %	214%	271%	466 %	214%

Table 5.4: Comparison of the eigenvalues

error in the calculation of the eigenvalues in the numerical model, and thus this is the reason these eigenvalues differ.

5.3.2 System test of dynamic response model

The dynamics response model can be tested as a system by comparing analytical results for the period and half-amplitude time with the resulting plots of the response. The analytical period for the phugoid and the damping for the spiral case are 46.5 and -8.4, following from the analytical eigenvalues indicated in table 5.4. As can be seen they match when they are compared with the numerical results in figure 4.2. This illustrates that there is most likely an error in the eigenvalue calculation by the simulation.

6. Validation

A Cessna Citation II aircraft is flown to obtain flight data to validate the simulation. Two sets of data where be gathered: static and dynamic measurements. In this chapter validation tests are discussed, followed by explaining how discrepancies were dealt with, finally a validation flow chart will be presented.

6.1 Optimization

The simulation data was tweaked by changing some stability coefficients, this resulted in a slightly better representation of the reality, however, the results (as will be explained thoroughly in section 6.3) are still far of from reality.

The stability coefficients that gave the best tweaking results were: C_{X_u} and C_{Z_u}. These resulted in the pitch rate and pitch angle to be nearly perfect for the short period motion and the phugoid motion while they were originally further off in phase and period.

6.2 Simulation Results and Validation Data

This section presents the validation data and the results of the simulation program after they have been improved with the first and second measurement series. This data is presented for five different motions in figures 6.1a through 6.3. The eigenvalues of the validation data for the short-period, phugoid and dutch-roll respectively are: $\lambda_s p = -0.0248 \pm 0.0674i$, $\lambda_p = -0.0001 \pm 0.0028i$ and $\lambda_d r = -0.0021 \pm 0.0487i$. The eigenvalues of the simulation tool short-period, phugoid and dutch-roll respectively are $-0.00231 + 0.104i$, $-0.00316 + 0.104i$ and $-0.215 + 1.92i$.

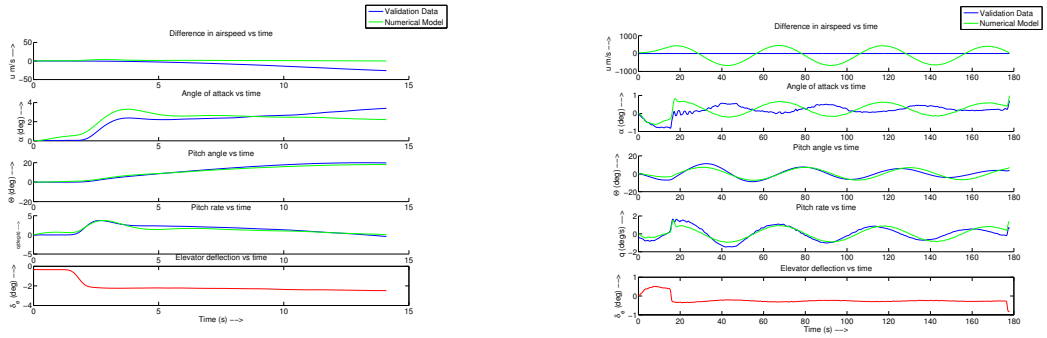

(a) The 5 response figures of a Short Period motion

(b) The 5 response figures of a Phugoid motion

Figure 6.1

6.3 Discussion of Validation Data

This section discusses the compares the data of a motion to the simulated response for that motion.

Short Period

When comparing the short period graphs it can be seen that they are quite similar. The Pitch rate and pitch angle are almost overlapping the validation data and is thus a good representation of real life. The angle of attack and the airspeed are deviating more towards the end of the motion. The code is for this not a very good representation of a real motion but can give an impression of the aircraft response.

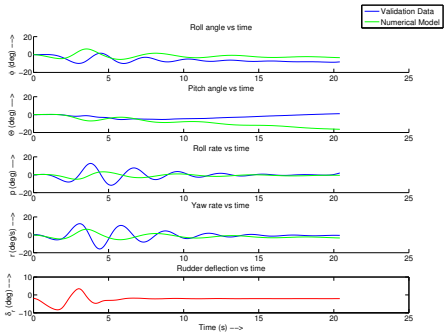

(a) The 5 response figures of a Dutch Roll motion

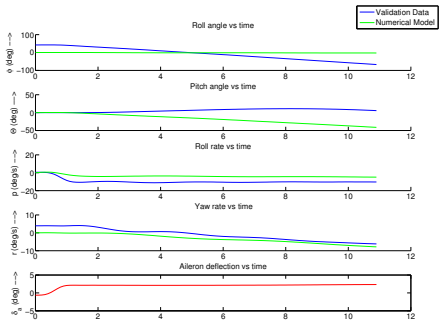

(b) The 5 response figures of a Aperiodic Roll motion

Figure 6.2

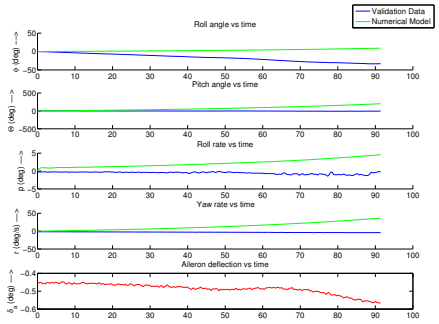

Figure 6.3: The 5 response figures of a Spiral motion

Phugoid
The phugoid motion is represented fairly well by the simulation of the pitch rate and the pitch angle. The airspeed is very much off, the numerical method gives an unreasonably large velocity, the program is not reliable for simulating this. The angle of attack is reasonably approached, but has a phase shift. For a later simulation program this could be improved.

Dutch Roll
The dutch roll simulation data is not very comparable to the real life data. The main reason is that the period is different which leads to a different motion. With more tweaking the program could become a better representation of reality. This was tried with trial and error, but can still improve more.

Aperiodic roll
The aperiodic motion is fairly well represented by the numerical model. The roll rate and yaw rate are very similar, with some more tweaking in the future the model may improve. The pitch angle for this case is not very well represented by the model, where the validation angle increases with time the numerical model decreases the pitch angle. This is thus not a good representation of reality.

Spiral
The spiral is also not very well represented by the simulation. the numerical model behaves to strong for the roll rate and yaw rate. The roll angle is not behaving strong enough while the roll rate is, so this is a strange and unreliable outcome.

6.4 Recommendations
The program can not be stated to be valid. Many of the values are far off, even after tweaking the program does not represent the reality very well. The simulation tool should therefore be re-evaluated completely and should than be re-tweaked. The data processing programs are verified to work correctly and can be used in the future without problems.

6.5 Discussion of Chosen Theory
The theory chosen for the first and second measurement series data processing was verified to be correct with expected values. This theory was thus a proper choice as it gave reliable outcomes. The theory used for the simulation tool should be reconsidered since the outcomes of the program were not validated. However, the tool

should first be further verified to check whether there are no programming errors.

7. Conclusion

The purpose of this simulation report was to cover the development and the final performance of a simulation model meant to predict the dynamic response of an aircraft to disturbances and control inputs. To validate this model with flight test data two other programs were developed to process the two measurement series of the prototype.

These data processing programs have been fully verified. The largest discrepancies that were detected for the first and second measurement series were 4% and 3.4% respectively and therefore it has been concluded that their performance is sufficient to use them for further development processes.

From the first measurement it was found that the current prototype has an Oswald efficiency factor of 0.8124 and a zero lift drag coefficient of 0.025. These values are within the expected range. From the second measurement series it was concluded that the prototype has currently both stick free static longitudinal as well as trim stability. Moreover, it also has control force stability.

The simulation model itself however was found to have improper performance. From the verification of this model it was found that the deviations in the eigenvalues predicted by the model from the analytically calculated eigenvalues are in the range of 140% to 3781%. This huge error is due to the wrong implementation of the eigenvalue calculation.

Another potential cause of the lacking performance of the simulation model is the poor piece of code creating the comparison for validation. Due to a poor program structure, a lack of variable and unit overview, the program quickly grew into an uncontrollable size and incomprehensible structure, halting progress in validation activities. The recommendation is to make a detailed flowchart for the program to have an overview of the data flow and then build the assembly code on that plan. Verification activities also have to be planned for this code.

Bibliography

[1] Antonio Filippone. *Data and performances of selected aircraft and rotorcraft*. 2000.

[2] Lambert. *Jane's All the World's Aircraft*. 1993.

[3] Jr Loftin, LK. *Quest for Performance, The Evolution of Modern Aircraft*. 1985.

[4] J.A. Mulder. *Flight Dynamics Lecture Notes*. 2013.

[5] University of Sydney. Properties of the atmosphere, -.

[6] D.P. Raymer. *Aircraft Design: A Conceptual Approach Fourth Edition*. 2015.

Appendix: group organisation

This section describes the group organisation of this report. It includes the amount of hours spent per person for each work package.

Table 7.1: Work division of technical report

Name/Work Package	Analytical Solution	Numerical Solution	Verification	Validation	Programming	Reporting	Total
Jasper Hemmes	20	6	8	6	11	5	56
Karl Kajak	8	11	15	3	8	6	51
Robert Koster	12	5	3	5	8	10	42
Boris Mulder	15	10	6	7	8	6	52
Christel Prins	8	15	10	8	6	8	55
Nichsan Rasappu	8	5	5		26	6	50